Performance Analysis of IRS-Assisted Multi-Cell Data and Energy Integrated Networks

Bingxin Zhang, *Member, IEEE,* Kun Yang, *Fellow, IEEE,* Kezhi Wang, *Senior Member, IEEE,* and Guopeng Zhang

***Abstract*—Intelligent reflecting surface (IRS) can significantly enhance the performance of data and energy integrated networks (DEIN) by adjusting its amplitude and/or phase. However, there is a lack of comprehensive performance analysis model for realistic DEIN where multiple cells exist rather than only one cell as assumed by most existing work. In this paper, we consider an IRS-assisted multi-cell DEIN. Specifically, in the downlink wireless energy transfer (WET) stage, the hybrid access point (HAP) in each cell broadcasts radio frequency (RF) energy signals to edge user equipments (UEs). Subsequently, during the uplink wireless information transfer (WIT) stage, the edge UEs employ the harvested energy to send their information to the HAP. We first represent the statistical characteristics of the signal-to-interference-plus-noise ratio (SINR) at the edge UE. Then, we derive the closed-form expressions for outage probability, ergodic rate and average symbol error probability of the edge UE in the typical cell. To gain more insights, we obtain the minimum required number of reflection elements and a sub-optimal solution for time allocation coefficients. Finally, extensive numerical results are provided to validate the correctness of the theoretical results.**

***Index Terms*—Intelligent reflecting surface (IRS), data and energy integrated network (DEIN), wireless energy transfer (WET), multi-cell, performance analysis.**

I. Introduction

THE Internet of Everything (IoE) aims to seamlessly integrate devices, humans, and data into a borderless ecosystem, enabling in an unprecedented era of intelligence and collaboration [1]. Due to cost and size considerations, the majority of IoE devices utilize limited-capacity embedded batteries as their energy source. Nevertheless, to sustain the regular operation of the devices, their batteries may be replaced frequently, resulting in substantial maintenance costs. Currently, radio frequency (RF)-based wireless energy transfer (WET) technology has been extensively studied to enhance the life-span of IoE devices. Combining traditional wireless information transfer (WIT) with WET yields a novel data and energy integrated network (DEIN) [2], which holds considerable promise for achieving energy sustainability in future 6G. In a DEIN, IoE devices first harvest energy from the RF signals transmitted by a hybrid access point (HAP), and then utilize the harvested energy to send information.

Many studies have been conducted on DEIN [3]–[7]. In [3], the authors discussed the application of WET technology in unmanned aerial vehicle (UAV) communication with cell-free massive multiple-input multiple-output systems. The authors in [4] studied the relationship between the transmit power of multiple wireless sources and the overall error probability by jointly allocating power and blocklength. In [5], the authors analyzed the performance of DEIN employing a distributed battery-free access protocol and provided the corresponding design guideline. The authors in [6] carefully designed the energy signal waveform in a DEIN to achieve energy sustainable communication for low-power devices. In [7], the authors analyzed the performance of a DEIN under the Rician fading model using age of information as an evaluation indicator. Nevertheless, as millimeter waves and even higher frequency bands are increasingly utilized in the DEIN, RF energy signals become highly vulnerable to obstruction by various obstacles, including trees and buildings. Consequently, there is an urgent demand for innovative technology to tackle this challenge.

The intelligent reflective surface (IRS), as an emerging technology, presents a promising approach to mitigating the aforementioned challenges. This is attributed to its capability to establish virtual links between the transmitter and receiver, thereby enhancing the performance of systems [8]–[10]. At present, IRS-assisted wireless communications have been widely studied in [11]–[22]. The authors in [11] analyzed the impact of imperfect hardware on the IRS-assisted multi-user communication system and given some new design insights. In [12], the authors discussed a new user-IRS association problem in the distributed IRSs-aided downlink communication. In [13], the authors characterized key performance indicators such as achievable spatial throughput of a heterogeneous wireless network by considering the random deployment of BSs and IRSs. The authors in [14] provided a generalized rate-splitting multiple access framework to study the outage probability of the IRS-aided downlink communication system. The authors in [15] investigated an IRS-assisted high-mobility communication system. Specifically, the remote BS utilized the intelligent refracting surface deployed on the top of vehicles to communicate with passengers inside high-speed vehicles. In [16], the authors proposed an IRS-mesh back-

This paper was partly funded by Jiangsu Major Project on Fundamental Researches (Grant No.: BK20243059), Gusu Innovation Project for People (Grant No.: ZXL2024360), Natural Science Foundation of China (Grant No. 62132004) and Nanjing University-China Mobile Communications Group Co.,Ltd. Joint Institute. (*Corresponding author: Kun Yang.*)

Bingxin Zhang and Kun Yang are with the State Key Laboratory of Novel Software Technology, Nanjing University, Nanjing 210008, China, and School of Intelligent Software and Engineering, Nanjing University (Suzhou Campus), Suzhou, 215163, China (email: bxzhang@nju.edu.cn; kunyang@nju.edu.cn).

Kezhi Wang is with Department of Computer Science, Brunel University London, Uxbridge, Middlesex, UB8 3PH (email: kezhi.wang@brunel.ac.uk).

Guopeng Zhang is with the School of Computer Science and Technology, China University of Mining and Technology, Xuzhou 221116, China (e-mail: gpzhang@cumt.edu.cn).

TABLE I
CONTRASTING THE CONTRIBUTIONS OF THIS WORK TO THE RELEVANT LITERATURE ON IRS.

Contributions	**This work**	[11]	[12]	[13]	[16]	[23]	[24]	[25]	[26]
Wireless information transfer	√	√	√	√	√	√	√	√	√
Wireless energy transfer	√					√	√	√	√
Multi-IRS	√		√	√	√		√		
Outage Probability	√				√				√
Ergodic rate	√	√							
Average symbol error probability	√								
Multi-cell co-channel interference	√		√	√					
Minimum required number of reflecting elements	√		√						
Optimal time allocation coefficients	√								

hauling architecture to overcome severe attenuation in high-frequency situations. The authors in [17] and [18] respectively attempted to optimize the performance of IRS-aided wireless communication systems utilizing deep Q-network and federated learning methods. Unlike the aforementioned research, the authors in [19] and [20] conducted extensive performance evaluations on IRS-aided wireless communication systems in finite blocklength regime, such as average error probability and average rate. In [21] and [22], the authors investigated the application of IRS in visible light communication systems to address the line-of-sight (LoS) blockage issue and enhance system performance.

Furthermore, many studies have shown that IRS can significantly improve the performance of DEIN [23]–[25], [27]–[32]. In [27], the authors considered the IRS as a wireless powered device. The IRS harvests energy from the RF signals broadcasted by the access point and then assists users in receiving information. In [23], the authors optimized the weighted sum-power harvested by energy users and the weighted sum-rate of information users in an active IRS-assisted simultaneous wireless information and power transfer system. The authors in [28] studied an IRS-assisted DEIN from the perspective of whether IRS is active or passive, and revealed the optimal deployment strategy for the active IRS. The authors in [24] considered an IRS-aided wireless-powered mobile edge computing system, and solved the problem of sum computing rate maximization by using energy beamforming and multi-user detection technology. The authors in [29] considered an IRS-assisted full-duplex DEIN, where the hybrid node sends information signals to multiple devices in the downlink transmission stage and receives energy signals from a power station in the uplink transmission stage. In [30], the authors investigated an additional passive beamforming gain provided by IRS on output direct current power, and proposed solutions for waveform and beamforming design of single-user and multi-user WET systems. The authors in [31] addressed an issue of whether different IRS phase shifts are required during the downlink WET and uplink WIT stages to reduce additional signaling overhead and computational complexity. Furthermore, to improve the sum throughput of an IRS-assisted DEIN, a dynamic IRS beamforming framework was proposed in [32]. The authors in [25] optimized the phase shift matrix of the IRS and the precoding matrix of the BS to maximize the weighted sum rate of information receivers while ensuring the energy harvesting requirement of the energy receivers. However, most of the current research on IRS-assisted DEIN systems involves using traditional convex optimization methods or converting non-convex problems into convex ones to optimize key parameters, including transmit power, precoding matrices, phase shifts of reflecting elements, etc. Yet, there is little literature conducting in-depth performance analysis of the system. Specifically, in a multi-cell scenario, there is scarce research that simultaneously considers the impact of neighboring cells on user equipments (UEs) of the typical cell in both energy harvesting and data transmission aspects.

Against the above background, we construct a IRS-assisted multi-cell DEIN, as shown in Fig 1. Table I summarizes the key characteristics of this work compared to typical IRS-assisted communication systems in existing literature [11]–[13], [16], [23]–[26]. Specifically, the main contributions are summarized as follows:

• Firstly, a IRS-aided multi-cell DEIN is investigated in this paper. We consider that, during the downlink WET stage, each cell's HAP broadcasts RF energy signals for edge UEs. During the uplink WIT stage, the edge UEs use the harvested energy to transmit their information to the HAP. In the considered system, the uplink information transmission capacity of the edge UE in the typical cell is enhanced by the energy received from adjacent cells during the downlink WET stage. However, during the uplink WIT stage, co-frequency interference from adjacent cells may lead to a decline in the ergodic capacity performance for the edge UE in the typical cell.

• Furthermore, due to the involvement of multiple random variables in the expression of the instantaneous signal-to-interference-plus-noise ratio (SINR), obtaining its exact statistical features directly is challenging. To this end, we approximate each random variable as a Gamma distribution and then utilize this approximation to analyze the statistical characteristics of SINR. Subsequently, we provide a comprehensive performance analysis of the edge UE in the typical cell, including outage probability, ergodic rate and average symbol error probability (ASEP). In addition, we derive the

minimum required number of reflecting elements and a sub-optimal time allocation coefficient for a given SINR threshold.

• Finally, numerical results obtained through Monte-Carlo simulations validate the accuracy of our theoretically derived results. Specifically, the system performance experiences a significant enhancement with an increase in the deployed number of reflecting elements, while it undergoes a notable reduction with an increase in the number of cells.

The rest of this paper is outlined as follows. In Section II, the system model with IRS assisted multi-cell DEIN is introduced. Section III conducts the closed-form expressions for outage probability, ergodic rate and ASEP. Section IV analyzes the minimum required number of elements and the sub-optimal time allocation coefficient for a given SINR threshold. Numerical results are presented in Section V to validate the correctness of theoretical analysis results. Finally, Section VI concludes this paper.

II. System Model

As shown in Fig. 1, we investigate a generic IRS-assisted multi-cell DEIN, which consists of M cells. In each cell, a HAP serves the single-antenna UEs within the cell with the assistance of an IRS. This paper focuses primarily on UEs at the cell edges to avoid complex analysis of interference among multiple UEs within the same cell. This focus allows us to better evaluate the impact of inter-cell interference on energy harvesting and data transmission and to derive tractable analytical results and insights. We assume that the connection between the HAP and edge UEs can only be established through the use of IRS, as there is a high probability that the direct links may be blocked by obstacles such as trees or buildings. Each HAP and IRS is equipped with a single-antenna and N passive reflecting elements, respectively. We represent the sets of HAPs and reflecting elements per IRS as $\mathcal{M} \triangleq \{1, 2, ..., M\}$ and $\mathcal{N} \triangleq \{1, 2, ..., N\}$, respectively.

Assuming each UE is equipped with a rechargeable batter/capacitor and an energy harvesting circuit component that can store the harvested energy to power its operation [33]. Therefore, in this paper, a 'harvest-then-transmit' two-stage protocol is considered, namely the downlink WET and the uplink WIT stage. In the downlink WET stage, edge UEs first harvest energy from the RF signals transmitted by the HAP. And then, in the uplink WIT stage, these edge UEs utilize the harvested energy to send their own data to the HAP. It should be noted that as shown in Fig. 1, the edge UE in the typical cell m may receive energy signals from adjacent cells during the downlink WET stage. Similarly, the edge UE of adjacent cells may cause interference to the edge UE in the typical cell m while sending their data. In other words, on the one hand, energy from adjacent cells enhances the uplink date transmission capacity for the edge UE in the typical cell m. On the other hand, the co-frequency interference from adjacent cells during the uplink WIT stage may result in a degradation of the ergodic capacity performance for the edge UE in the typical cell m.

To maximize the reflection gain and avoid the implementation cost associated with simultaneously controlling both the reflection amplitude and phase, we assume that the reflection amplitude of each element of the IRS is set to 1 [9]. We also consider that the signal from any HAP to any edge UE is reflected at most once by the IRS, as multiple reflections through the IRS would lead to significant signal attenuation due to the multiplicative path-loss of the reflection links. We assume that the HAP can obtain perfect channel state information (CSI) for the edge UE within the same cell [12] [19]. Note that the assumption of perfect CSI implies that the HAP must periodically send training information for channel estimation, which may reduce overall bandwidth efficiency. In practice, the considered edge UEs could be stationary, meaning that the CSI might remain relatively constant over long periods. Consequently, frequent channel estimation may not be required. In addition, we also assume that the HAP is unable to obtain the CSI of edge UEs in adjacent cells, as these UEs are not its service targets.

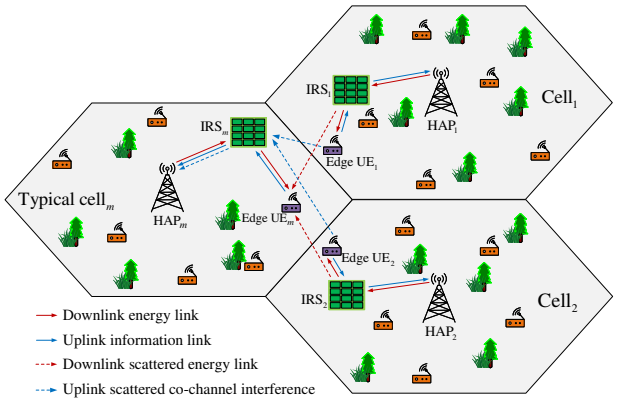

Fig. 1. An IRS-assisted multi-cell DEIN model.

A. The Downlink WET Stage

In the downlink WET stage, the complex channels from the HAP m to the IRS m, from the IRS m to the edge UE m and from the IRS i of the adjacent cell to the edge UE m are denoted by $\mathbf{g}_m^{\mathrm{E}} = \left[g_{m,1}^{\mathrm{E}}, ..., g_{m,N}^{\mathrm{E}}\right]^{\mathrm{H}} \in \mathbb{C}^{1\times N}$, $\mathbf{h}_m^{\mathrm{E}} = \left[h_{m,1}^{\mathrm{E}}, ..., h_{m,N}^{\mathrm{E}}\right] \in \mathbb{C}^{N\times 1}$ and $\mathbf{f}_i^{\mathrm{E}} = \left[f_{i,1}^{\mathrm{E}}, ..., f_{i,N}^{\mathrm{E}}\right] \in \mathbb{C}^{N\times 1}$, respectively. We assume that the channel between the HAP and the n-th IRS's element is a LoS channel, as both the HAP and IRS are usually deployed at relatively high positions [34]. Therefore, according to [34], one has $|g_{m,n}^{\mathrm{E}}| = 1$. Furthermore, the channel between the n-th IRS's element and edge UEs include both LoS and non-LoS (NLoS) fading, that is, experiencing Rician fading channel. Similarly, assuming that the energy transmission channel propagated by adjacent cells through the IRS scattering during the downlink WET phase is also modeled as a Rician fading channel. Therefore, $h_{m,n}^{\mathrm{E}}$ and $f_{i,n}^{\mathrm{E}}$ can be modeled as

$$h_{m,n}^{\mathrm{E}} = \sqrt{\frac{\kappa_m^{\mathrm{E}}}{1+\kappa_m^{\mathrm{E}}}}\bar{h}_{m,n}^{\mathrm{E}} + \sqrt{\frac{1}{1+\kappa_m^{\mathrm{E}}}}\tilde{h}_{m,n}^{\mathrm{E}}, \tag{1}$$

$$f_{i,n}^{\mathrm{E}} = \sqrt{\frac{\kappa_i^{\mathrm{E}}}{1+\kappa_i^{\mathrm{E}}}}\bar{f}_{i,n}^{\mathrm{E}} + \sqrt{\frac{1}{1+\kappa_i^{\mathrm{E}}}}\tilde{f}_{i,n}^{\mathrm{E}}, \tag{2}$$

where κ_m^{E} and κ_i^{E} respectively denote the Rician factors of the channels between the IRS and the edge UE in the typical cell m, and between the IRS of adjacent cell i and the edge UE in the typical cell m. Furthermore, $\bar{h}_{m,n}^{\mathrm{E}}$ and $\bar{f}_{i,n}^{\mathrm{E}}$ are the LoS components, $\tilde{f}_{i,n}^{\mathrm{E}}$ and $\tilde{f}_{i,n}^{\mathrm{E}}$ are the NLoS components following complex Gaussian distribution with zero mean and unit variance. It is worth noting that since HAP i and IRS k belong to different cells and are not deployed with mutual coordination, their channel may be affected by obstacles or scatterers. The channel between HAP m and IRS k can be modeled as a Rician channel with both LoS and NLoS components. Therefore, the inter-cell link between HAP i and IRS m is significantly weaker than the intra-cell link between HAP i and IRS i. Furthermore, the IRS is typically deployed near the UE or HAP, positioned between them to maximize system performance. This results in the distance from UE i to IRS i to HAP m being greater than the distance form UE i to IRS i to HAP m. Consequently, during the WIT stage, the double fading effect of the links from UE i to IRS i to HAP m are likely much stronger than that of the links from UE i to IRS m to HAP m, $\forall i \in \mathcal{M}, i \neq m$. Therefore, we did not consider the links from UE i to IRS i to HAP m when analyzing the system performance.

As a result, in the downlink WET phase, the received signal of the edge UE in the typical cell m can be written as

$$y_m^{\mathrm{E}} = \sqrt{P_{m,\mathrm{T}}\beta_{m,\mathrm{BR}}^{\mathrm{E}}\beta_{m,\mathrm{RU}}^{\mathrm{E}}}\left(\mathbf{h}_m^{\mathrm{E}}\right)^{\mathrm{H}}\mathbf{\Phi}_m^{\mathrm{E}}\mathbf{g}_m^{\mathrm{E}}x_m^{\mathrm{E}} + \sum_{i\in\mathcal{M},i\neq m}\sqrt{P_{i,\mathrm{T}}\beta_{i,\mathrm{BR}}^{\mathrm{E}}\beta_{i,\mathrm{RU}}^{\mathrm{E}}}\left(\mathbf{f}_i^{\mathrm{E}}\right)^{\mathrm{H}}\mathbf{\Phi}_i^{\mathrm{E}}\mathbf{g}_i^{\mathrm{E}}x_i^{\mathrm{E}} + n_m^{\mathrm{E}}, \tag{3}$$

where $(\cdot)^{\mathrm{H}}$ denotes the conjugate transpose of a vector/matrix, $P_{m,\mathrm{T}}$ is the transmit power of the HAP in cell m, x_m^{E} denotes the information symbol with $\mathbb{E}\{||x_m^{\mathrm{E}}||^2\} = 1$ and $n_m^{\mathrm{E}} \sim \mathcal{CN}(0,\sigma_m^2)$ is the additive white Gaussian noise (AWGN) at the UE m. $\beta_{m,u}^{\mathrm{E}} = d_{m,u}^{-\alpha_{m,u}}$ is the large-scale fading coefficient determined by the propagation distance, where $d_{m,u}$ denotes the transmission distance, $\alpha_{m,u}$ denotes the path-loss exponent, $u \in \{\mathrm{BR},\mathrm{RU}\}$. In addition, $\mathbf{\Phi}_m^{\mathrm{E}} = \mathrm{diag}(e^{j\phi_{m,1}^{\mathrm{E}}},...,e^{j\phi_{m,N}^{\mathrm{E}}})$ denotes the diagonal phase shifting matrix of the IRS in cell m during the downlink WET stage, $\phi_{m,n}^{\mathrm{E}} \in [0,2\pi)$ is the phase shifting of the n-th reflecting element of the IRS in the cell m. In order to maximize the energy received by the edge UE m during the downlink WET stage, the phase shifts of all elements are adjusted to be aligned with the edge UE it serves, i.e., $\phi_{m,n}^{\mathrm{E}} = -\arg(h_{m,n}^{\mathrm{E}}) - \arg(g_{m,n}^{\mathrm{E}}), \forall n \in \{1,...,N\}$.

The energy harvested by the edge UE in the typical cell m during the downlink WET stage can be expressed as

$$E_m = \eta\tau^{\mathrm{E}}P_{m,\mathrm{T}}\beta_{m,\mathrm{BR}}^{\mathrm{E}}\beta_{m,\mathrm{RU}}^{\mathrm{E}}\left|\left(\mathbf{h}_m^{\mathrm{E}}\right)^{\mathrm{H}}\mathbf{\Phi}_m^{\mathrm{E}}\mathbf{g}_m^{\mathrm{E}}\right|^2 + \sum_{i\in\mathcal{M},i\neq m}\eta\tau^{\mathrm{E}}p_{i,\mathrm{T}}\beta_{i,\mathrm{BR}}^{\mathrm{E}}\beta_{i,\mathrm{RU}}^{\mathrm{E}}\left|\left(\mathbf{f}_i^{\mathrm{E}}\right)^{\mathrm{H}}\mathbf{\Phi}_i^{\mathrm{E}}\mathbf{g}_i^{\mathrm{E}}\right|^2, \tag{4}$$

where $\eta \in (0,1)$ is the energy conversion efficiency of UEs and τ^{E} denotes the duration of the downlink WET stage for each edge UE.

B. The Uplink WIT Stage

In the uplink WIT stage, the complex channels from the IRS m to the HAP m, from the edge UE m to the IRS m and from the UE i of the adjacent cell to the IRS m are denoted by $\mathbf{g}_m^{\mathrm{I}} = \left[g_{m,1}^{\mathrm{I}},...,g_{m,N}^{\mathrm{I}}\right]^{\mathrm{H}} \in \mathbb{C}^{1\times N}$, $\mathbf{h}_m^{\mathrm{I}} = \left[h_{m,1}^{\mathrm{I}},...,h_{m,N}^{\mathrm{I}}\right] \in \mathbb{C}^{N\times 1}$ and $\mathbf{f}_i^{\mathrm{I}} = \left[f_{i,1}^{\mathrm{I}},...,f_{i,N}^{\mathrm{I}}\right] \in \mathbb{C}^{N\times 1}$, respectively. Similar to the downlink WET channel model, one has $|g_{m,n}^{\mathrm{I}}| = 1$ [34]. Furthermore, $h_{m,n}^{\mathrm{I}}$ and $f_{i,n}^{\mathrm{I}}$ can be represented as

$$h_{m,n}^{\mathrm{I}} = \sqrt{\frac{\kappa_m^{\mathrm{I}}}{1+\kappa_m^{\mathrm{I}}}}\bar{h}_{m,n}^{\mathrm{I}} + \sqrt{\frac{1}{1+\kappa_m^{\mathrm{I}}}}\tilde{h}_{m,n}^{\mathrm{I}}, \tag{5}$$

$$f_{i,n}^{\mathrm{I}} = \sqrt{\frac{\kappa_i^{\mathrm{I}}}{1+\kappa_i^{\mathrm{I}}}}\bar{f}_{i,n}^{\mathrm{I}} + \sqrt{\frac{1}{1+\kappa_i^{\mathrm{I}}}}\tilde{f}_{i,n}^{\mathrm{I}}, \tag{6}$$

where κ_m^{I} and κ_i^{I} respectively denote the Rician factors of the channels between the IRS and the edge UE in the typical cell m, and between the IRS m and the adjacent edge UE i. In particular, $\bar{h}_{m,n}^{\mathrm{E}}$ and $\bar{f}_{i,n}^{\mathrm{E}}$ are the LoS components, $\tilde{f}_{i,n}^{\mathrm{E}}$ and $\tilde{f}_{i,n}^{\mathrm{E}}$ correspond to the NLoS components.

In the uplink WIT stage, the edge UE in each cell utilizes the energy harvested during the dowlink WET stage to transmit data to their HAP within a duration of τ^{I}, satisfying $\tau^{\mathrm{E}}+\tau^{\mathrm{I}} = 1$. Therefore, according to (4), the average transmit power of the edge UE in the typical cell m can be written as

$$p_m = \frac{\eta\tau^{\mathrm{E}}}{\tau^{\mathrm{I}}}P_{m,\mathrm{T}}\beta_{m,\mathrm{BR}}^{\mathrm{E}}\beta_{m,\mathrm{RU}}^{\mathrm{E}}\left|\left(\mathbf{h}_m^{\mathrm{E}}\right)^{\mathrm{H}}\mathbf{\Phi}_m^{\mathrm{E}}\mathbf{g}_m^{\mathrm{E}}\right|^2 + \sum_{i\in\mathcal{M},i\neq m}\frac{\eta\tau^{\mathrm{E}}}{\tau^{\mathrm{I}}}P_{i,\mathrm{T}}\beta_{i,\mathrm{BR}}^{\mathrm{E}}\beta_{i,\mathrm{RU}}^{\mathrm{E}}\left|\left(\mathbf{f}_i^{\mathrm{E}}\right)^{\mathrm{H}}\mathbf{\Phi}_i^{\mathrm{E}}\mathbf{g}_i^{\mathrm{E}}\right|^2. \tag{7}$$

Similar to the downlink WET phase, we also omitted the links from UE k to IRS k to HAP m, $\forall k \in \mathcal{M}, k \neq m$, during the uplink WIT phase. Thus, the signal received during the uplink WIT phase at the HAP in typical cell m can be represented

$$y_m^{\mathrm{I}} = \sqrt{p_m\beta_{m,\mathrm{RB}}^{\mathrm{I}}\beta_{m,\mathrm{UR}}^{\mathrm{I}}}\left(\mathbf{g}_m^{\mathrm{I}}\right)^{\mathrm{H}}\mathbf{\Phi}_m^{\mathrm{I}}\mathbf{h}_m^{\mathrm{I}}x_m^{\mathrm{I}} + \sum_{k\in\mathcal{M},k\neq m}\sqrt{p_k\beta_{m,\mathrm{RB}}^{\mathrm{I}}\beta_{k,\mathrm{UR}}^{\mathrm{I}}}\left(\mathbf{g}_m^{\mathrm{I}}\right)^{\mathrm{H}}\mathbf{\Phi}_m^{\mathrm{I}}\mathbf{f}_k^{\mathrm{I}}x_k^{\mathrm{I}} + n_m^{\mathrm{I}}, \tag{8}$$

where x_m^{I} is the at symbol with $\mathbb{E}\{||x_m^{\mathrm{I}}||^2\} = 1$, n_m^{I} denotes the AWGN at the HAP of cell m the follows zero mean and variance of σ_m^{I}. Especially, $\beta_{m,\mathrm{RB}}^{\mathrm{I}}$, $\beta_{m,\mathrm{UR}}^{\mathrm{I}}$ and $\beta_{k,\mathrm{UR}}^{\mathrm{I}}$ are the large-scale fading coefficients between the IRS and HAP in the cell m, between the UE and IRS in the cell m, and between the UE in the adjacent cell k and the IRS in the cell m during the uplink WIT stage, respectively. Moreover, $\mathbf{\Phi}_m^{\mathrm{I}} = \mathrm{diag}(e^{j\phi_{m,1}^{\mathrm{I}}},...,e^{j\phi_{m,N}^{\mathrm{I}}})$ denotes the diagonal phase shifting matrix of the IRS in cell m during the uplink WIT stage, where $\phi_{m,n}^{\mathrm{I}} \in [0,2\pi)$ and $\phi_{m,n}^{\mathrm{I}} = -\arg(h_{m,n}^{\mathrm{I}}) - \arg(g_{m,n}^{\mathrm{I}}), \forall n \in \{1,...,N\}$.

Then, the instantaneous SINR at the HAP of the typical cell m is given by

$$\gamma_m = \frac{p_m\beta_{m,\mathrm{RB}}^{\mathrm{I}}\beta_{m,\mathrm{UR}}^{\mathrm{I}}\left|\left(\mathbf{g}_m^{\mathrm{I}}\right)^{\mathrm{H}}\mathbf{\Phi}_m^{\mathrm{I}}\mathbf{h}_m^{\mathrm{I}}\right|^2}{\sum_{k\in\mathcal{M},k\neq m}p_k\beta_{m,\mathrm{RB}}^{\mathrm{I}}\beta_{k,\mathrm{UR}}^{\mathrm{I}}\left|\left(\mathbf{g}_m^{\mathrm{I}}\right)^{\mathrm{H}}\mathbf{\Phi}_m^{\mathrm{I}}\mathbf{f}_k^{\mathrm{I}}\right|^2 + \sigma_m^2}. \tag{9}$$

Subsequently, by defining $\delta_m^{\mathrm{E}} = P_{m,\mathrm{T}}\beta_{m,\mathrm{BR}}^{\mathrm{E}}\beta_{m,\mathrm{RU}}^{\mathrm{E}}$, $\delta_i^{\mathrm{E}} = P_{i,\mathrm{T}}\beta_{i,\mathrm{BR}}^{\mathrm{E}}\beta_{i,\mathrm{RU}}^{\mathrm{E}}$, $\delta_m^{\mathrm{I}} = \beta_{m,\mathrm{RB}}^{\mathrm{I}}\beta_{m,\mathrm{UR}}^{\mathrm{I}}$ and $\delta_k^{\mathrm{I}} = \beta_{m,\mathrm{RB}}^{\mathrm{I}}\beta_{k,\mathrm{UR}}^{\mathrm{I}}$, we can restate γ_m as shown in (10) at the bottom of this page.

Based on (10), the uplink achievable rate R_m (bit/s/Hz) of the edge UE in the typical cell m can be given by

$$R_m = \log_2\left(1+\gamma_m\right). \tag{11}$$

III. Performance Analysis

In this section, we conduct the performance of the IRS-aided multi-cell DEIN system. Three performance evaluation metrics are investigated, namely outage probability, ergodic rate, and ASEP.

For the sake of simplicity, we introduce the following variables substitutions. Based on (10), one has $X = \delta_m^{\mathrm{E}}\left|\left(\mathbf{h}_m^{\mathrm{E}}\right)^{\mathrm{H}}\mathbf{\Phi}_m^{\mathrm{E}}\mathbf{g}_m^{\mathrm{E}}\right|^2$, $Y = \sum_{i\in\mathcal{M},i\neq m}\delta_i^{\mathrm{E}}\left|\left(\mathbf{f}_i^{\mathrm{E}}\right)^{\mathrm{H}}\mathbf{\Phi}_i^{\mathrm{E}}\mathbf{g}_i^{\mathrm{E}}\right|^2$, $Z = X+Y$, $L = \delta_m^{\mathrm{I}}\left|\left(\mathbf{g}_m^{\mathrm{I}}\right)^{\mathrm{H}}\mathbf{\Phi}_m^{\mathrm{I}}\mathbf{h}_m^{\mathrm{I}}\right|^2$, $\Omega = ZL$, $U_k = \delta_k^{\mathrm{E}}\left|\left(\mathbf{h}_k^{\mathrm{E}}\right)^{\mathrm{H}}\mathbf{\Phi}_k^{\mathrm{E}}\mathbf{g}_k^{\mathrm{E}}\right|^2 + \sum_{j\in\mathcal{M},j\neq k}\delta_j^{\mathrm{E}}\left|\left(\mathbf{f}_j^{\mathrm{E}}\right)^{\mathrm{H}}\mathbf{\Phi}_j^{\mathrm{E}}\mathbf{g}_j^{\mathrm{E}}\right|^2$, $V_k = \delta_k^{\mathrm{I}}\left|\left(\mathbf{g}_m^{\mathrm{I}}\right)^{\mathrm{H}}\mathbf{\Phi}_m^{\mathrm{I}}\mathbf{f}_k^{\mathrm{I}}\right|^2$ and $I = \sum_{k\in\mathcal{M},k\neq m}U_kV_k$.

The SINR of edge UE in the typical cell m can be rewritten as

$$\gamma_m = \frac{\left(X+Y\right)L}{\sum_{k\in\mathcal{M},k\neq m}U_kV_k + \frac{\sigma_m^2\tau^{\mathrm{I}}}{\eta\tau^{\mathrm{E}}}} = \frac{ZL}{I+\Lambda} = \frac{\Omega}{I+\Lambda}, \tag{12}$$

where $\Lambda = \frac{\sigma_m^2\tau^{\mathrm{I}}}{\eta\tau^{\mathrm{E}}}$. Next, we derive the CDF and PDF of the random variables Z and L, respectively.

In order to obtain a tractable statistical characteristic expression for γ_m, this paper utilizes the moment-matching method to approximate the random variable Z as a Gamma distribution. To this end, we need to derive the first and second moments of Z. Due to X and Y are independent, one has

$$\mathbb{E}\left[Z\right] = \mathbb{E}\left[X\right] + \mathbb{E}\left[Y\right], \tag{13}$$

$$\mathbb{E}\left[Z^2\right] = \mathbb{E}\left[X^2\right] + 2\mathbb{E}\left[X\right]\mathbb{E}\left[Y\right] + \mathbb{E}\left[Y^2\right]. \tag{14}$$

We further derive the first and second moments for the random variables X and Y. Let $\zeta = \left|\left(\mathbf{h}_m^{\mathrm{E}}\right)^{\mathrm{H}}\mathbf{\Phi}_m^{\mathrm{E}}\mathbf{g}_m^{\mathrm{E}}\right|^2$ and assume that the HAP m can obtain sufficient CSI. In order to maximize the received SINR, the IRS m should carefully configure its phase shifts to compensate for channel phases, i.e., $\phi_{m,n}^{\mathrm{E}} = -\arg(h_{m,n}^{\mathrm{E}}) - \arg(g_{m,n}^{\mathrm{E}})$. Then, according to the results obtained in Corollary 1 of our previous work [35], one can know that ζ should follow a non-central chi-square distribution with two degrees of freedom under the optimal phase shift configuration, i.e., $\zeta \sim \mathcal{X}^2\left(2, \sqrt{\frac{\kappa_m^{\mathrm{E}}}{1+\kappa_m^{\mathrm{E}}}}N, \frac{N}{2(\kappa_m^{\mathrm{E}}+1)}\right)$. Following the statistical characteristics of the non-central chi-square distribution, one can easily obtain $\mathbb{E}\left[X\right] = \delta_m^{\mathrm{E}}\left(2\sigma^2+s^2\right)$ and $\mathbb{E}\left[X^2\right] = \left(\delta_m^{\mathrm{E}}\right)^2\left(4\sigma^4+4\sigma^2s^2+2\sigma^2+s^2\right)$, where $s = \sqrt{\frac{\kappa_m^{\mathrm{E}}}{1+\kappa_m^{\mathrm{E}}}}N$ and $\sigma^2 = \frac{N}{2(1+\kappa_m^{\mathrm{E}})}$.

Let $\varrho_i = \left|\left(\mathbf{f}_i^{\mathrm{E}}\right)^{\mathrm{H}}\mathbf{\Phi}_i^{\mathrm{E}}\mathbf{g}_i^{\mathrm{E}}\right|^2$. Then, for the random variable Y, $\mathbb{E}\left[Y\right]$ can be rewritten as

$$\mathbb{E}\left[Y\right] = \mathbb{E}\left[\sum_{i=1,i\neq m}^{M}\delta_i^{\mathrm{E}}\left|\left(\mathbf{f}_i^{\mathrm{E}}\right)^{\mathrm{H}}\mathbf{\Phi}_i^{\mathrm{E}}\mathbf{g}_i^{\mathrm{E}}\right|^2\right] = \sum_{i=1,i\neq m}^{M}\delta_i^{\mathrm{E}}\mathbb{E}\left[\varrho_i\right]. \tag{15}$$

Based on the results obtained in our previous work [35], one can have

$$\left(\sqrt{\frac{\kappa^{\mathrm{E}}}{1+\kappa^{\mathrm{E}}}}\bar{\mathbf{f}}_i^{\mathrm{E}} + \sqrt{\frac{1}{1+\kappa^{\mathrm{E}}}}\tilde{\mathbf{f}}_i^{\mathrm{E}}\right)^{\mathrm{H}}\mathbf{\Phi}_i^{\mathrm{E}}\bar{\mathbf{g}}_i^{\mathrm{E}} \sim \mathcal{CN}\left(0, \frac{N}{2}\right). \tag{16}$$

As a result, $\mathbb{E}\left[\varrho_i\right]$ can be derived as

$$\mathbb{E}\left[\varrho_i\right] = \mathbb{E}\left[\left|\left(\sqrt{\frac{\kappa^{\mathrm{E}}}{1+\kappa^{\mathrm{E}}}}\bar{\mathbf{f}}_i^{\mathrm{E}} + \sqrt{\frac{1}{1+\kappa^{\mathrm{E}}}}\tilde{\mathbf{f}}_i^{\mathrm{E}}\right)^{\mathrm{H}}\mathbf{\Phi}_i^{\mathrm{E}}\bar{\mathbf{g}}_i^{\mathrm{E}}\right|^2\right] = N. \tag{17}$$

Then, based on (15) and (17), one has $\mathbb{E}\left[Y\right] = \sum_{i=1,i\neq m}^{M}\delta_i^{\mathrm{E}}N$.

$\mathbb{E}\left[Y^2\right]$ can be rewritten as

$$\begin{aligned}\mathbb{E}\left[Y^2\right] &= \mathbb{E}\left[\left(\sum_{i=1,i\neq m}^{M}\delta_i^{\mathrm{E}}\left|\left(\mathbf{f}_i^{\mathrm{E}}\right)^{\mathrm{H}}\mathbf{\Phi}_i^{\mathrm{E}}\mathbf{g}_i^{\mathrm{E}}\right|^2\right)^2\right] \\ &= \sum_{i=1,i\neq m}^{M}\left(\delta_i^{\mathrm{E}}\right)^2\mathbb{E}\left[\varrho_i^2\right] + \sum_{i=1,i\neq m}^{M}\sum_{j=1,j\neq i}^{M}\delta_i^{\mathrm{E}}\delta_j^{\mathrm{E}}\mathbb{E}\left[\varrho_i\right]\mathbb{E}\left[\varrho_j\right].\end{aligned} \tag{18}$$

Based on (16), one has

$$\begin{aligned}\mathbb{E}\left[\varrho_i^2\right] &= \mathbb{E}\left[\left|\left(\mathbf{f}_i^{\mathrm{E}}\right)^{\mathrm{H}}\mathbf{\Phi}_i^{\mathrm{E}}\mathbf{g}_i^{\mathrm{E}}\right|^4\right] \\ &= \mathbb{E}\left[\left|\left(\sqrt{\frac{\kappa^{\mathrm{E}}}{1+\kappa^{\mathrm{E}}}}\bar{\mathbf{f}}_i^{\mathrm{E}} + \sqrt{\frac{1}{1+\kappa^{\mathrm{E}}}}\tilde{\mathbf{f}}_i^{\mathrm{E}}\right)^{\mathrm{H}}\mathbf{\Phi}_i^{\mathrm{E}}\bar{\mathbf{g}}_i^{\mathrm{E}}\right|^4\right] = 2N^2.\end{aligned} \tag{19}$$

Then, by substituting (17) and (19) into (18), one can have that $\mathbb{E}\left[Y^2\right] = \sum_{i=1,i\neq m}^{M}2\left(\delta_i^{\mathrm{E}}\right)^2N^2 + \sum_{i=1,i\neq m}^{M}\sum_{j=1,j\neq i}^{M}\delta_i^{\mathrm{E}}\delta_j^{\mathrm{E}}N^2$. By substituting $\mathbb{E}\left[X\right]$, $\mathbb{E}\left[X^2\right]$, $\mathbb{E}\left[Y\right]$ and $\mathbb{E}\left[Y^2\right]$ into (13) and (14), respectively, $\mathbb{E}\left[Z\right]$ and $\mathbb{E}\left[Z^2\right]$ can be obtained.

By exploiting a moment matching method, Z can be approximated as a Gamma random variable with the following parameters $\beta_Z = \frac{\left(\mathbb{E}[Z]\right)^2}{\mathbb{E}[Z^2]-\left(\mathbb{E}[Z]\right)^2}$ and $\theta_Z = \frac{\mathbb{E}\left[Z^2\right]-\left(\mathbb{E}[Z]\right)^2}{\mathbb{E}[Z]}$, where β_Z denotes the shape parameter and θ_Z denotes the scale parameter. Based on the definition of Gamma distribution, the CDF of Z can be expressed as

$$F_Z(z) = \frac{1}{\Gamma(\beta_Z)}\Upsilon\left(\beta_Z, \frac{z}{\theta_Z}\right), \tag{20}$$

$$\gamma_m = \frac{\left(\delta_m^{\mathrm{E}}\left|\left(\mathbf{h}_m^{\mathrm{E}}\right)^{\mathrm{H}}\mathbf{\Phi}_m^{\mathrm{E}}\mathbf{g}_m^{\mathrm{E}}\right|^2 + \sum_{i\in\mathcal{M},i\neq m}\delta_i^{\mathrm{E}}\left|\left(\mathbf{f}_i^{\mathrm{E}}\right)^{\mathrm{H}}\mathbf{\Phi}_i^{\mathrm{E}}\mathbf{g}_i^{\mathrm{E}}\right|^2\right)\delta_m^{\mathrm{I}}\left|\left(\mathbf{g}_m^{\mathrm{I}}\right)^{\mathrm{H}}\mathbf{\Phi}_m^{\mathrm{I}}\mathbf{h}_m^{\mathrm{I}}\right|^2}{\sum_{k\in\mathcal{M},k\neq m}\left(\delta_k^{\mathrm{E}}\left|\left(\mathbf{h}_k^{\mathrm{E}}\right)^{\mathrm{H}}\mathbf{\Phi}_k^{\mathrm{E}}\mathbf{g}_k^{\mathrm{E}}\right|^2 + \sum_{j\in\mathcal{M},j\neq k}\delta_j^{\mathrm{E}}\left|\left(\mathbf{f}_j^{\mathrm{E}}\right)^{\mathrm{H}}\mathbf{\Phi}_j^{\mathrm{E}}\mathbf{g}_j^{\mathrm{E}}\right|^2\right)\delta_k^{\mathrm{I}}\left|\left(\mathbf{g}_m^{\mathrm{I}}\right)^{\mathrm{H}}\mathbf{\Phi}_m^{\mathrm{I}}\mathbf{f}_k^{\mathrm{I}}\right|^2 + \frac{\sigma_m^2\tau^{\mathrm{I}}}{\eta\tau^{\mathrm{E}}}}, \tag{10}$$

where $\Gamma(\cdot)$ denotes the gamma function and $\Upsilon(\cdot,\cdot)$ is the lower incomplete Gamma function.

Similar to the random variable ζ, the cascaded channel gain during the uplink WIT phase also follows a non-central chi-square distribution with two degrees of freedom. To this end, we again use the moment-matching method to approximate L as a Gamma distribution. Therefore, the PDF of L can be expressed as

$$f_L(x) = \frac{1}{\Gamma(\beta_L)\theta_L^{\beta_L}} x^{\beta_L - 1} e^{-\frac{x}{\theta_L}}, \tag{21}$$

where $\beta_L = \frac{(\mathbb{E}[L])^2}{\mathbb{E}[L^2]-(\mathbb{E}[L])^2}$ and $\theta_L = \frac{\mathbb{E}\left[L^2\right]-(\mathbb{E}[L])^2}{\mathbb{E}[L]}$. Specifically, the derivation process for $\mathbb{E}[L]$ and $\mathbb{E}\left[L^2\right]$ is similar to that of $\mathbb{E}[Z]$ and $\mathbb{E}\left[Z^2\right]$.

Then, based on (20) and (21), as well as the conclusion from Lemma 1 in our previous work [36], we can derive the PDF of the random variable Ω as

$$f_\Omega(x) = \frac{2x^{\frac{\beta_Z+\beta_L}{2}-1}}{\Gamma(\beta_Z)\Gamma(\beta_L)\left(\theta_Z\theta_L\right)^{\frac{\beta_Z+\beta_L}{2}}} K_{\beta_L-\beta_Z}\left(2\sqrt{\frac{x}{\theta_Z\theta_L}}\right), \tag{22}$$

where $K_\vartheta(\cdot)$ is the ϑ-th order modified Bessel function of the second kind.

Unfortunately, it is difficult to obtain the CDF of Ω by integrating (22). To this end, we use the following method to derive the CDF of the random variable Ω.

$$\begin{aligned}
F_\Omega(x) &= \Pr\left\{Z < \frac{x}{L}\right\} = \int_0^\infty F_Z\left(\frac{x}{t}\right) f_L(t)\mathrm{d}t \\
&= \frac{1}{\Gamma(\beta_Z)\Gamma(\beta_L)\theta_L^{\beta_L}} \int_0^\infty t^{\beta_L-1} e^{-\frac{t}{\theta_L}} \Upsilon\left(\beta_Z, \frac{x}{\theta_Z t}\right) \mathrm{d}t \\
&\overset{y=\frac{1}{t}}{=} \frac{1}{\Gamma(\beta_Z)\Gamma(\beta_L)\theta_L^{\beta_L}} \int_0^\infty y^{-\beta_L-1} e^{-\frac{1}{y\theta_L}} \Upsilon\left(\beta_Z, \frac{xy}{\theta_Z}\right) \mathrm{d}y \\
&\overset{(a)}{=} \frac{\theta_L^{-\beta_L}}{\Gamma(\beta_Z)\Gamma(\beta_L)} \int_0^\infty y^{-\beta_L-1} G_{1,0}^{0,1}\left(y\theta_L \left|{}^{1}_{\cdot}\right.\right) G_{1,2}^{1,1}\left(\frac{xy}{\theta_Z}\left|{}^{1}_{\beta_Z,0}\right.\right) \mathrm{d}y \\
&\overset{(b)}{=} \frac{\theta_L}{\Gamma(\beta_Z)\Gamma(\beta_L)} \int_0^\infty G_{1,0}^{0,1}\left(y\theta_L \left|{}^{-\beta_L}_{\cdot}\right.\right) G_{1,2}^{1,1}\left(\frac{xy}{\theta_Z}\left|{}^{1}_{\beta_Z,0}\right.\right) \mathrm{d}y \\
&\overset{(c)}{=} \frac{1}{\Gamma(\beta_Z)\Gamma(\beta_L)} G_{1,3}^{2,1}\left(\frac{x}{\theta_Z\theta_L}\left|{}^{1}_{\beta_L,\beta_Z,0}\right.\right),
\end{aligned} \tag{23}$$

where $G_{m,n}^{p,q}\left[x\left|{}^{a_1,\ldots,a_p}_{b_1,\ldots,b_q}\right.\right]$ denotes the Meijer's G-function, (a) is obtained by using [37, Eq. (8.4.3.2), Eq. (8.4.16.1)], (b) follows from [38, Eq. (9.31.5)] and (c) is obtained by using [38, Eq. (7.811.1)].

Similar to the random variables Z and L, we also approximate the variable I as a Gamma distribution. Now, we derive $\mathbb{E}[I]$ and $\mathbb{E}\left[I^2\right]$. According to the statistical independence of random variables U_k and V_k, one has

$$\mathbb{E}[I] = \sum_{k\in\mathcal{M},k\neq m} \mathbb{E}[U_k]\,\mathbb{E}[V_k], \tag{24}$$

$$\begin{aligned}
\mathbb{E}\left[I^2\right] &= \mathbb{E}\left[\left(\sum_{k\in\mathcal{M},k\neq m} U_k V_k\right)^2\right] \\
&= \sum_{k\in\mathcal{M},k\neq m} \mathbb{E}\left[U_k^2\right]\mathbb{E}\left[V_k^2\right] \\
&\quad + \sum_{k\in\mathcal{M},k\neq m}\sum_{i\in\mathcal{M},i\neq k} \mathbb{E}[U_k]\,\mathbb{E}[V_k]\,\mathbb{E}[U_i]\,\mathbb{E}[V_i],
\end{aligned} \tag{25}$$

where the derivation process of $\mathbb{E}\left[U_k^2\right]$, $\mathbb{E}\left[V_k^2\right]$, $\mathbb{E}[U_k]$ and $\mathbb{E}[V_k]$ are similar to (15) and (18).

Therefore, by using the moment matching method, the PDF of the random variable I can be represented as

$$f_I(x) = \frac{1}{\Gamma(\beta_I)\theta_I^{\beta_I}} x^{\beta_I-1} e^{-\frac{x}{\theta_I}}, \tag{26}$$

where $\beta_I = \frac{(\mathbb{E}[I])^2}{\mathbb{E}[I^2]-(\mathbb{E}[I])^2}$ and $\theta_I = \frac{\mathbb{E}\left[I^2\right]-(\mathbb{E}[I])^2}{\mathbb{E}[I]}$.

Next, we derive the statistical characteristics of γ_m in (12). One has the following lemma.

Lemma 1. The CDF of γ_m in (12) can be expressed as

$$\begin{aligned}
&F_{\gamma_m}(x) = \\
&\frac{1}{\Gamma(\beta_{\mathrm{Z}})\Gamma(\beta_{\mathrm{L}})\Gamma(\beta_{\mathrm{I}})} \sum_{q=1}^{Q} \mathcal{W}_q \mathcal{S}_q^{\beta_{\mathrm{I}}-1} G_{2,3}^{2,2}\left(\frac{x\theta_I\mathcal{S}_q + x\Lambda}{\theta_Z\theta_L}\left|{}^{1}_{\beta_{\mathrm{L}},\beta_{\mathrm{Z}},0}\right.\right),
\end{aligned} \tag{27}$$

where $\mathcal{W}_q$ and $\mathcal{S}_q$ are respectively the weights of the Laguerre polynomial and the sample points, tabulated in [39, Table. (25.9)]. Specifically, x_q is the q-th zero of Laguerre polynomial $L_Q(x_q)$ and the corresponding the q-th weight factor is given by $\mathcal{W}_q = \frac{(Q!)^2 x_q}{(Q+1)^2[L_{Q+1}(x_q)]^2}$.

Proof: Based on (12), (23) and (26), one has

$$\begin{aligned}
F_{\gamma_m}(x) &= \Pr\left\{\frac{\Omega}{I+\Lambda} < x\right\} = \int_0^\infty F_\Omega(xt + x\lambda) f_I(t)\mathrm{d}t \\
&= \frac{\theta_I^{-\beta_{\mathrm{I}}}}{\Gamma(\beta_{\mathrm{Z}})\Gamma(\beta_{\mathrm{L}})\Gamma(\beta_{\mathrm{I}})} \int_0^\infty t^{\beta_{\mathrm{I}}-1} e^{-\frac{t}{\theta_{\mathrm{I}}}} \\
&\qquad \times G_{1,3}^{2,1}\left(\frac{xt + x\Lambda}{\theta_Z\theta_L}\left|{}^{1}_{\beta_{\mathrm{L}},\beta_{\mathrm{Z}},0}\right.\right) \mathrm{d}t.
\end{aligned} \tag{28}$$

Unfortunately, it is difficult to directly obtain an exact closed-form expression for the above integration. To this end, we provide an approximate closed-form expression for γ_m by applying the Gaussian Laguerre integration method [39]. The obtained result is shown in (27). ■

Remark 1. In general, the AWGN power σ_m at the HAP is a very small quantity, thus the constant interference term Λ in formula (12) can be ignored compared to the interference of edge UEs in adjacent cells. Ignoring the constant Λ, one

can obtain another CDF for γ_m as follows

$$\begin{aligned} F_{\gamma_m}(x) &= \Pr\{\Omega < xI\} = \int_0^\infty F_\Omega(xt) f_I(t) \mathrm{d}t \\ &= \frac{\theta_I^{-\beta_I}}{\Gamma(\beta_Z)\Gamma(\beta_L)\Gamma(\beta_I)} \int_0^\infty t^{\beta_I - 1} e^{-\frac{t}{\theta_I}} \\ &\qquad \times G_{1,3}^{2,1}\left(\frac{xt}{\theta_Z\theta_L}\Big|_{\beta_L,\beta_Z,0}^{1}\right) \mathrm{d}t \\ &\overset{(a)}{=} \frac{1}{\Gamma(\beta_Z)\Gamma(\beta_L)\Gamma(\beta_I)} G_{2,3}^{2,2}\left(\frac{\theta_I x}{\theta_Z\theta_L}\Big|_{\beta_L,\beta_Z,0}^{1-\beta_I,1}\right), \end{aligned} \tag{29}$$

where (a) is obtained by using [37, Eq. (8.4.3.2)] and [38, Eq. (9.31.5), Eq. (7.811.1)].

In order to obtain traceable results, we employ the conclusion in Remark 1 to derive the closed-form expressions for the three performance metrics of the system, namely outage probability, ergodic rate and ASEP.

Remark 2. In particular, when there is only one cell in the IRS-assisted DEIN, i.e., $M = 1$, the edge UE is no longer subject to energy signals and co-channel interference from neighboring cells. At this point, the instantaneous signal-to-noise ratio (SNR) at the HAP can be expressed as

$$\begin{aligned} \gamma_0 &= \Lambda_0 \delta_0^{\mathrm{E}} \delta_0^{\mathrm{I}} \left| \left(\mathbf{h}_0^{\mathrm{E}}\right)^{\mathrm{H}} \mathbf{\Phi}_0^{\mathrm{E}} \mathbf{g}_0^{\mathrm{E}} \right|^2 \left| \left(\mathbf{g}_0^{\mathrm{I}}\right)^{\mathrm{H}} \mathbf{\Phi}_0^{\mathrm{I}} \mathbf{h}_0^{\mathrm{I}} \right|^2 \\ &= \Lambda_0 X_0 L_0 = \Lambda_0 \Omega_0, \end{aligned} \tag{30}$$

where $\Lambda_0 = \frac{\eta \tau^{\mathrm{E}}}{\sigma_0^2 \tau^{\mathrm{I}}}$, $\delta_0^{\mathrm{E}} = P_{0,\mathrm{T}} \beta_{0,\mathrm{BR}}^{\mathrm{E}} \beta_{0,\mathrm{RU}}^{\mathrm{E}}$, $\delta_0^{\mathrm{I}} = \beta_{0,\mathrm{RB}}^{\mathrm{I}} \beta_{0,\mathrm{UR}}^{\mathrm{I}}$, $X_0 = \delta_0^{\mathrm{E}} \left| \left(\mathbf{h}_0^{\mathrm{E}}\right)^{\mathrm{H}} \mathbf{\Phi}_0^{\mathrm{E}} \mathbf{g}_0^{\mathrm{E}} \right|^2$, $L_0 = \delta_0^{\mathrm{I}} \left| \left(\mathbf{g}_0^{\mathrm{I}}\right)^{\mathrm{H}} \mathbf{\Phi}_0^{\mathrm{I}} \mathbf{h}_0^{\mathrm{I}} \right|^2$ and $\Omega_0 = X_0 L_0$.

In this case, the random variables X_0 and L_0 can be approximated as a Gamma distribution similar to Z, respectively. Therefore, the CDF of γ_0 can be derived as

$$F_{\gamma_0}(x) = \frac{1}{\Gamma(\beta_{X_0})\Gamma(\beta_{L_0})} G_{1,3}^{2,1}\left(\frac{x}{\theta_{X_0}\theta_{L_0}\Lambda_0}\Big|_{\beta_{L_0},\beta_{X_0},0}^{1}\right), \tag{31}$$

where $\beta_{X_0} = \frac{(\mathbb{E}[X_0])^2}{\mathbb{E}[X_0^2]-(\mathbb{E}[X_0])^2}$, $\theta_{X_0} = \frac{\mathbb{E}[X_0^2]-(\mathbb{E}[X_0])^2}{\mathbb{E}[X_0]}$, $\beta_{L_0} = \frac{(\mathbb{E}[L_0])^2}{\mathbb{E}[L_0^2]-(\mathbb{E}[L_0])^2}$ and $\theta_{L_0} = \frac{\mathbb{E}[L_0^2]-(\mathbb{E}[L_0])^2}{\mathbb{E}[L_0]}$. Specifically, the derivation process is similar to (23).

A. Outage probability

Lemma 2. Based on (29), the closed-form expression of outage probability for the edge UE in typical cell m can be approximated as

$$P_m^{\mathrm{O}} = \frac{1}{\Gamma(\beta_Z)\Gamma(\beta_L)\Gamma(\beta_I)} G_{2,3}^{2,2}\left(\frac{\theta_I\left(2^{R_{\mathrm{th}}}-1\right)}{\theta_Z\theta_L}\Big|_{\beta_L,\beta_Z,0}^{1-\beta_I,1}\right), \tag{32}$$

where R_{th} denotes the achievable rate threshold.

Proof: For a given rate threshold R_{th}, based on the definition of the outage probability, one has

$$\begin{aligned} P_m^{\mathrm{O}} &= \Pr\{\log_2(1+\gamma_m) < R_{\mathrm{th}}\} \\ &= \Pr\left\{\gamma_m < 2^{R_{\mathrm{th}}} - 1\right\} = F_{\gamma_m}\left(2^{R_{\mathrm{th}}} - 1\right) \\ &= \frac{1}{\Gamma(\beta_{\mathrm{Z}})\Gamma(\beta_{\mathrm{L}})\Gamma(\beta_{\mathrm{I}})} G_{2,3}^{2,2}\left(\frac{\theta_I\left(2^{R_{\mathrm{th}}}-1\right)}{\theta_Z\theta_L}\Big|_{\beta_{\mathrm{L}},\beta_{\mathrm{Z}},0}^{1-\beta_{\mathrm{I}},1}\right). \end{aligned} \tag{33}$$

Here, the proof is completed. ■

Remark 3. By using the result obtained from Lemma 1, a more precise expression of outage probability for the edge UE in the typical cell m can be written as

$$\begin{aligned} P_m^{\mathrm{O}} &= \frac{1}{\Gamma(\beta_{\mathrm{Z}})\Gamma(\beta_{\mathrm{L}})\Gamma(\beta_{\mathrm{I}})} \times \\ &\quad \sum_{q=1}^{Q} \mathcal{W}_q \mathcal{S}_q^{\beta_{\mathrm{I}}-1} G_{2,3}^{2,2}\left(\frac{\left(2^{R_{\mathrm{th}}}-1\right)\left(\theta_I \mathcal{S}_q + \Lambda\right)}{\theta_Z\theta_L}\Big|_{\beta_{\mathrm{L}},\beta_{\mathrm{Z}},0}^{1}\right), \end{aligned} \tag{34}$$

where Q, $\mathcal{W}_q$ and $\mathcal{S}_q$ are defined in (27).

B. Ergodic rate

Lemma 3. Based on (11) and (29), the closed-form expression of ergodic rate for the edge UE in the typical cell m can be derived as

$$R_m = \frac{1}{\Gamma(\beta_Z)\Gamma(\beta_L)\Gamma(\beta_I)\ln 2} G_{5,6}^{4,4}\left(\frac{\theta_I}{\theta_Z\theta_L}\Big|_{0,0,\beta_L,\beta_Z,0,1}^{0,1-\beta_I,1,0,1}\right). \tag{35}$$

Proof: Please refer to Appendix A. ■

C. Average symbol error probability

To further investigate the performance of the IRS assisted multi-cell DEIN, we aim to evaluate the ASEP of the edge UE in the typical cell m. The generic ASEP expression for various modulation schemes can be given by [40]

$$\bar{P}_e = \varphi \mathbb{E}\left[Q\left(\sqrt{\varsigma\gamma_m}\right)\right] = \varphi \int_0^\infty Q\left(\sqrt{\varsigma t}\right) f_{\gamma_m}(t) \mathrm{d}t, \tag{36}$$

where φ and ς are the modulation parameters, and $Q(x) = \frac{1}{\sqrt{2\pi}} \int_x^\infty e^{\frac{t^2}{2}} \mathrm{d}t$ denotes the Gaussian Q-function. Then, one has the following lemma.

Lemma 4. The closed-form expression of ASEP for the edge UE in the typical cell m can be derived as

$$\bar{P}_e = \frac{\varphi}{2\sqrt{\pi}\Gamma(\beta_Z)\Gamma(\beta_L)\Gamma(\beta_I)} G_{5,5}^{2,5}\left(\frac{2\theta_I}{\varsigma\theta_Z\theta_L}\Big|_{\beta_L,\beta_Z,0,1,0}^{1,\frac{1}{2},1-\beta_I,1,0}\right). \tag{37}$$

Proof: Please refer to Appendix B. ■

IV. Two Extended Analyses

In this section, we aim to reveal some valuable insights into the considered IRS-assisted network. For this purpose, we conduct theoretical analysis to characterize the minimum required number of IRS's reflecting elements N and the sub-optimal time allocation coefficient τ^{E} for a given SINR threshold $\gamma_{m,\mathrm{th}}$. To this end, we first study the average SINR performance of the edge UE in the typical cell m.

The average SINR of the edge UE in the typical cell m can be expressed as

$$\tilde{\gamma}_m = \mathbb{E}\left[\gamma_m\right] = \mathbb{E}\left[\frac{\Omega}{I+\Lambda}\right]. \tag{38}$$

Unfortunately, it is difficult to directly obtain a closed-form expression for the average SINR in (38). To further derive a

traceable result, we apply Jensen's inequality to obtain a lower bound on the average SINR as shown below,

$$\tilde{\gamma}_m = \mathbb{E}\left[\frac{\Omega}{I+\Lambda}\right] = \mathbb{E}\left[\Omega\right]\mathbb{E}\left[\frac{1}{I+\Lambda}\right] \geq \frac{\mathbb{E}\left[\Omega\right]}{\mathbb{E}\left[I\right]+\Lambda} = \bar{\gamma}_m. \tag{39}$$

Then, we characterize the expectations of the random variables Ω and I. Similar to the derivation process of (13), the expectations of Ω and I can be derived as

$$\begin{aligned}\mathbb{E}\left[\Omega\right] &= \mathbb{E}\left[Z\right]\mathbb{E}\left[L\right] = \left(\mathbb{E}\left[X\right]+\mathbb{E}\left[Y\right]\right)\mathbb{E}\left[L\right] \\ &= \frac{\delta_m^{\mathrm{E}}\delta_m^{\mathrm{I}}N^2 + \delta_m^{\mathrm{E}}\delta_m^{\mathrm{I}}\left(\kappa_m^{\mathrm{E}}+\kappa_m^{\mathrm{I}}\right)N^3 + \delta_m^{\mathrm{E}}\delta_m^{\mathrm{I}}\kappa_m^{\mathrm{E}}\kappa_m^{\mathrm{I}}N^4}{\left(1+\kappa_m^{\mathrm{E}}\right)\left(1+\kappa_m^{\mathrm{I}}\right)} \\ &\quad + \frac{\sum_{i\in\mathcal{M},i\neq m}\delta_i^{\mathrm{E}}\delta_m^{\mathrm{I}}N^2 + \sum_{i\in\mathcal{M},i\neq m}\delta_i^{\mathrm{E}}\delta_m^{\mathrm{I}}\kappa_m^{\mathrm{I}}N^3}{1+\kappa_m^{\mathrm{I}}},\end{aligned} \tag{40}$$

$$\begin{aligned}\mathbb{E}\left[I\right] &= \sum_{k\in\mathcal{M},k\neq m}\mathbb{E}\left[U_k\right]\mathbb{E}\left[V_k\right] \\ &= \sum_{k\in\mathcal{M},k\neq m}\left(\frac{\delta_k^{\mathrm{E}}\left(N+\kappa_k^{\mathrm{E}}N^2\right)}{1+\kappa_k^{\mathrm{E}}} + \sum_{j\in\mathcal{M},j\neq k}N\delta_j^{\mathrm{E}}\right)\delta_k^{\mathrm{I}}N \\ &= \sum_{k\in\mathcal{M},k\neq m}\frac{\delta_k^{\mathrm{E}}\delta_k^{\mathrm{I}}N^2 + \delta_k^{\mathrm{E}}\delta_k^{\mathrm{I}}\kappa_k^{\mathrm{E}}N^3}{1+\kappa_k^{\mathrm{E}}} \\ &\quad + N^2\sum_{k\in\mathcal{M},k\neq m}\sum_{j\in\mathcal{M},j\neq k}\delta_j^{\mathrm{E}}\delta_k^{\mathrm{I}}.\end{aligned} \tag{41}$$

Next, let $\mu_1 = \frac{\delta_m^{\mathrm{E}}\delta_m^{\mathrm{I}}}{(1+\kappa_m^{\mathrm{E}})(1+\kappa_m^{\mathrm{I}})}$, $\mu_2 = \frac{\delta_m^{\mathrm{E}}\delta_m^{\mathrm{I}}\left(\kappa_m^{\mathrm{E}}+\kappa_m^{\mathrm{I}}\right)}{(1+\kappa_m^{\mathrm{E}})(1+\kappa_m^{\mathrm{I}})}$, $\mu_3 = \frac{\delta_m^{\mathrm{E}}\delta_m^{\mathrm{I}}\kappa_m^{\mathrm{E}}\kappa_m^{\mathrm{I}}}{(1+\kappa_m^{\mathrm{E}})(1+\kappa_m^{\mathrm{I}})}$, $\mu_4 = \frac{\delta_m^{\mathrm{I}}\sum_{i\in\mathcal{M},i\neq m}\delta_i^{\mathrm{E}}}{1+\kappa_m^{\mathrm{I}}}$, $\mu_5 = \frac{\delta_m^{\mathrm{I}}\kappa_m^{\mathrm{I}}\sum_{i\in\mathcal{M},i\neq m}\delta_i^{\mathrm{E}}}{1+\kappa_m^{\mathrm{I}}}$, $\mu_6 = \sum_{k\in\mathcal{M},k\neq m}\frac{\delta_k^{\mathrm{E}}\delta_k^{\mathrm{I}}}{1+\kappa_k^{\mathrm{E}}}$, $\mu_7 = \sum_{k\in\mathcal{M},k\neq m}\frac{\delta_k^{\mathrm{E}}\delta_k^{\mathrm{I}}\kappa_k^{\mathrm{E}}}{1+\kappa_k^{\mathrm{E}}}$ and $\mu_8 = \sum_{k\in\mathcal{M},k\neq m}\sum_{j\in\mathcal{M},j\neq k}\delta_j^{\mathrm{E}}\delta_k^{\mathrm{I}}$, $\bar{\gamma}_m$ in (39) can be represented as

$$\bar{\gamma}_m = \frac{\mu_1N^2+\mu_2N^3+\mu_3N^4+\mu_4N^2+\mu_5N^3}{\mu_6N^2+\mu_7N^3+\mu_8N^2+\Lambda}. \tag{42}$$

In addition, as N is sufficiently large, i.e., $N\to\infty$, one has

$$\bar{\gamma}_m^{\infty} \to \mu_3N + \frac{\mu_2+\mu_5}{\mu_7} = \mathcal{O}\left(N\right). \tag{43}$$

It follows from (43) that as $N\to\infty$, the average SINR of the edge UE in the typical cell m will linearly increase with N due to the fourfold growth in the received signal power over surpassing the threefold growth in the interference power.

A. Minimum required number of elements N

In this subsection, we attempt to analyze the minimum required number of reflection elements for a given SINR threshold. Therefore, base on (42), the following inequality must be satisfied:

$$\frac{\left(\mu_1+\mu_4\right)N^2+\left(\mu_2+\mu_5\right)N^3+\mu_3N^4}{\left(\mu_6+\mu_8\right)N^2+\mu_7N^3+\Lambda} \geq \bar{\gamma}_{m,\mathrm{th}}, \tag{44}$$

To further simplify (44), one has

$$AN^4+BN^3+CN^2+D\geq 0, \tag{45}$$

where $A=\mu_3$, $B=\mu_2+\mu_5-\mu_7\bar{\gamma}_{m,\mathrm{th}}$, $C=\mu_1+\mu_4-\left(\mu_6+\mu_8\right)\bar{\gamma}_{m,\mathrm{th}}$ and $D=-\Lambda\bar{\gamma}_{m,\mathrm{th}}$.

Lemma 5. For a given SINR threshold, the minimum required number of reflecting elements to be satisfied is

$$N \geq \max\left\{\lceil x_1\rceil,\lceil x_2\rceil,\lceil x_3\rceil,\lceil x_4\rceil\right\}, \tag{46}$$

$$x_1 = \lambda_4-\lambda_5-\lambda_{6a}, \tag{46a}$$

$$x_2 = \lambda_4-\lambda_5+\lambda_{6a}, \tag{46b}$$

$$x_3 = \lambda_4+\lambda_5-\lambda_{6a}, \tag{46c}$$

$$x_4 = \lambda_4+\lambda_5+\lambda_{6a}, \tag{46d}$$

where $\lceil x\rceil$ denotes the ceiling operation for x, $\lambda_4 = -\frac{B}{4A}$, $\lambda_5 = \frac{1}{2}\sqrt{\lambda_2+\Delta_3}$, $\lambda_{6a} = \frac{1}{2}\sqrt{2\lambda_2-\Delta_3-\frac{\lambda_3}{8\lambda_5}}$, $\lambda_{6b} = \frac{1}{2}\sqrt{2\lambda_2-\Delta_3+\frac{\lambda_3}{8\lambda_5}}$, $\lambda_2 = \frac{B^2}{4A^2}-\frac{2C}{3A}$, $\lambda_3 = -\frac{B^3}{A^3}+\frac{4BC}{A^2}$, $\Delta_3 = \frac{\sqrt[3]{2}\Delta_1}{3A\lambda_1}+\frac{\lambda_1}{3\sqrt[3]{2}A}$, $\lambda_1 = \sqrt[3]{\Delta_2+\sqrt{-4\Delta_1^3+\Delta_2^2}}$, $\Delta_1 = C^2+12AD$ and $\Delta_2 = 2C^3+27B^2D-72ACD$.

Proof: Please refer to Appendix C. ■

B. Sub-optimal time allocation coefficient τ^{I}

According to the "harvest-then-transmit" protocol, it is evident that increasing the duration of downlink WET enables edge UEs to harvest more energy, but it reduces the duration of uplink WIT, leading to a decrease in the amount of data transmitted. Therefore, there exists a trade-off between the time allocation for uplink WET and downlink WIT. To gain further engineering insights, we investigate the optimal time allocation coefficients in this subsection.

Based on (10), (11) and (42), we define the ergodic capacity of edge UE in typical cell m during the uplink WIT phase as

$$C_m = \frac{\tau^{\mathrm{I}}}{\ln 2}\ln\left(1+\frac{\varepsilon_1}{\varepsilon_2+\frac{\varepsilon_3\tau^{\mathrm{I}}}{1-\tau^{\mathrm{I}}}}\right), \tag{47}$$

where $\varepsilon_1 = \mu_1N^2+\mu_2N^3+\mu_3N^4+\mu_4N^2+\mu_5N^3$, $\varepsilon_2 = \mu_6N^2+\mu_7N^3+\mu_8N^2$ and $\varepsilon_3 = \frac{\sigma_m^2}{\eta}$.

By observing (47), one can find that there must be an optimal τ^{I} that maximizes the ergodic capacity of the edge UE in the typical cell m. Unfortunately, we can not directly provide an analytical expression for the optimal τ^{I} due to the existence of the nonlinear natural logarithmic function $\ln(\cdot)$. Although it is easy to obtain a sub-optimal τ^{I} by utilizing some heuristic algorithms, such as genetic algorithms, particle swarm optimization algorithms, etc., this does not give more insights for engineering. To this end, when the number of IRS's elements is large enough, we utilize Taylor expansion technology to provide a sub-optimal solution for τ^{I}. One has the following lemma.

Lemma 6. When the number of IRS's elements is quite large, we can obtain a sub-optimal time allocation coefficient τ^{I} as follows to maximize the ergodic capacity of the edge UE in the typical cell.

$$\tau^{\mathrm{I}} = 1-\frac{1}{\sqrt{1+\frac{\varpi_1}{\varpi_2}}}, \tag{48}$$

where $\varpi_1 = \frac{1}{\ln 2}\ln\left(1+\frac{\varepsilon_1}{\varepsilon_2}\right)$ and $\varpi_2 = \frac{1}{\ln 2}\frac{\varepsilon_1\varepsilon_3}{\varepsilon_2^2\left(1+\frac{\varepsilon_1}{\varepsilon_2}\right)}$.

Proof: Please refer to Appendix D. ■

TABLE II
TABLE OF SIMULATION PARAMETERS.

Path-loss exponent α_i^{E} from the IRS in adjacent cell i to the edge UE in typical cell m	2.7
Path-loss exponent α_m^{E} from the HAP to the IRS (the IRS to the edge UE) in cell m	2.0 (2.4)
Time allocation coefficient τ^{E} in the downlink WET stage	0.4
The transmit power $P_{m,\mathrm{T}}$ of the HAP in cell m (dBm)	-30
The power of AWGN σ_m^2 at the HAP in cell m (dBm)	-94
The number of cells M in the studied network	3
The number of reflecting elements N in each IRS	8
Energy conversion efficiency of edge UEs η	0.85
The Rician factors κ_m^{E}, κ_i^{E}, κ_m^{I} and κ_i^{I} in the studied network	2

V. NUMERICAL RESULTS

In this section, we verify the effectiveness and accuracy of the derived numerical results through Monte-Carlo simulations. Unless otherwise specified, we summarize the main parameters adopted in Table I. We run 10^6 times of Monte-Carlo simulations in this paper. Especially, in Fig. 2 to Fig. 6, the curves labeled as 'Simulation' are obtained through Monte-Carlo simulations. The curves labeled as 'Analysis, appr1' and 'Analysis, ppr2' are obtained by using (27) and (29), respectively.

Fig. 2 shows the outage probability versus the required rate threshold for different values of reflecting elements at each IRS. One can see that under a given number of IRS's elements, the outage probability gradually increases as the threshold of required rate. This implies that as the rate requirements for edge UEs become more stringent, the probability of failing to meet these requirements increases. For the same rate threshold, a larger N leads to a lower outage probability due to the higher passive beamforming gain provided by the IRS. This phenomenon aligns with expectations and serves as a promising strategy for mitigating outage probability. It can be observed that the results derived using the Gaussian Laguerre integration method, namely 'Analysis, appr1', match very well with the simulation results. In addition, with the increased of reflecting elements, the accuracy of the results obtained by applying (29) is enhanced. This is because, with a sufficiently large N, the constant interference term Λ in formula (12) can be neglected.

In Fig. 3, we illustrate the outage probability versus the required rate for different numbers of cells in the network. Similar to Fig. 2, it is easy to observe that the outage probability increases with the required rate threshold. In Fig. 3, for any given rate threshold, one can see that the outage probability of increases significantly with the number of cells in the network. This is due to the interference caused by more edge UEs of adjacent cells, leading to a decrease in network performance.

Fig. 4 depicts the outage probability versus the transmit power $P_{m,\mathrm{T}}$ of the HAP with different numbers of IRS's elements. It can be seen that the curves corresponding to 'Analysis, appr2' do not change with the increase of $P_{m,\mathrm{T}}$. This is because the ignored constant term Λ includes the transmit power of the HAP. However, the curves corresponding to 'Analysis, appr1' first decrease, then tend to flatten, and finally coincide with the case of 'Analysis, appr2'. This implies that increasing the transmit power of each HAP is limited in reducing the outage probability of the edge UE. This is because when the transmit power of the HAP in each cell is increased simultaneously, although it enhances the energy harvested by edge UEs, it also results in stronger co-channel interference from neighboring cells. Furthermore, similar to Fig. 2, larger values of reflecting elements yields lower outage probability.

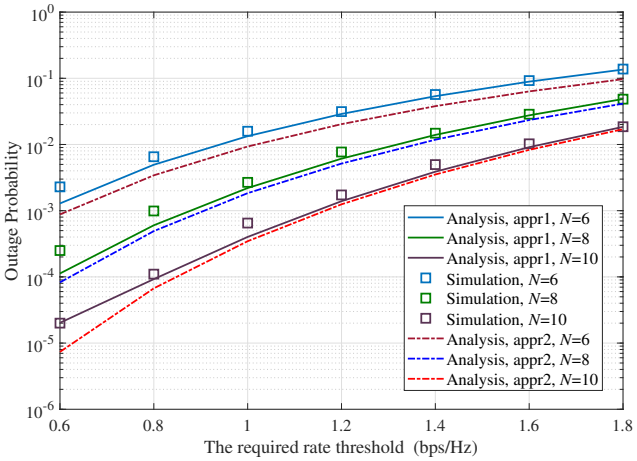

Fig. 2. The outage probability versus the required rate threshold for different values of N.

In Fig. 5, we plot the ergodic rate versus the number of reflecting elements for different values of M. It can be observed that the ergodic rate increases with the number of IRS's elements as expected. Moreover, it can be seen that for any fixed number of reflecting elements, the ergodic rate performance decreases with the increase in the number of cells in the network. This means that the negative impact of co-channel interference caused by the increase in the number of adjacent cells is higher than the positive effect of improving the energy harvested by the edge UE in the typical cell.

Fig 6 shows the ASEP versus the number of reflecting elements for different modulations. Specifically, Fig. 6 analyzes four modulation schemes, namely 32-ary quadrature amplitude

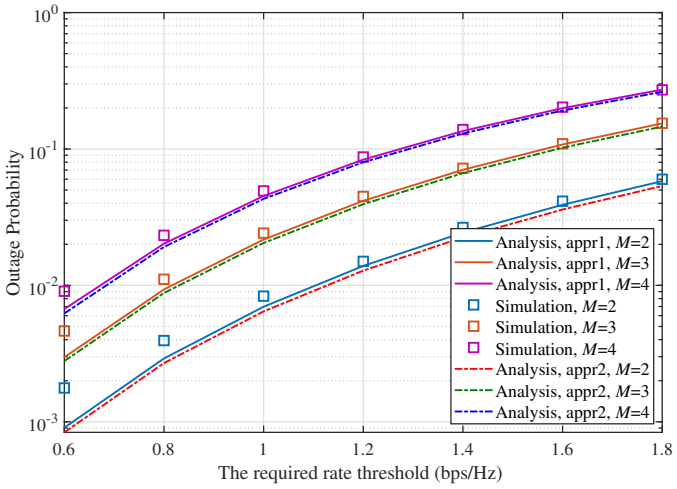

Fig. 3. The outage probability versus SINR for different values of M.

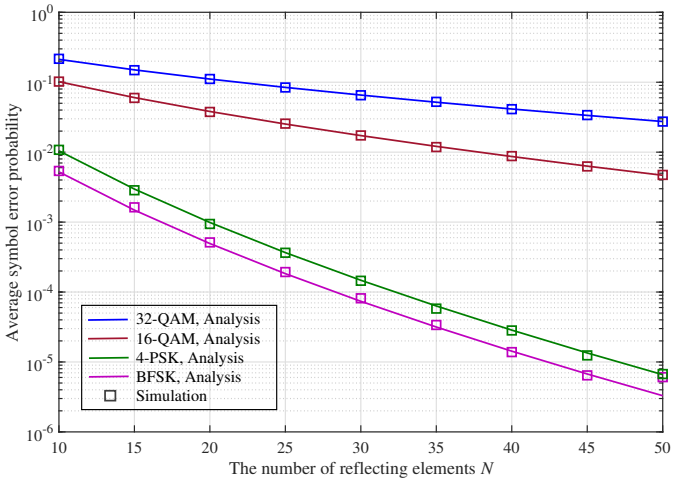

Fig. 6. The average symbol error probability versus the number of reflecting elements for different modulations.

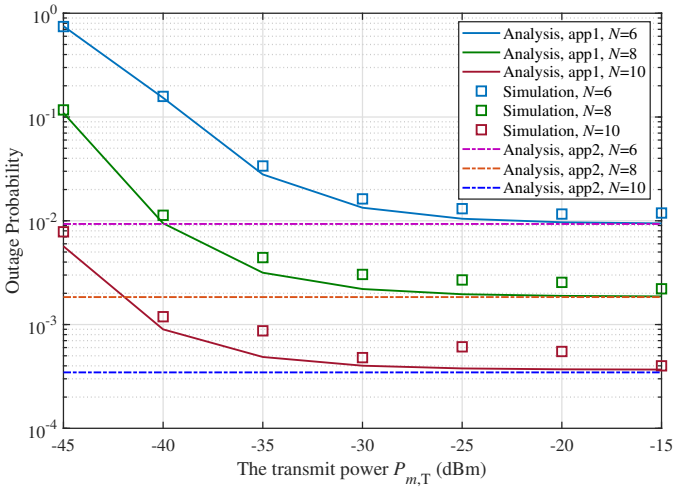

Fig. 4. The outage probability versus the transmit power $P_{m,\mathrm{T}}$ for different values of N.

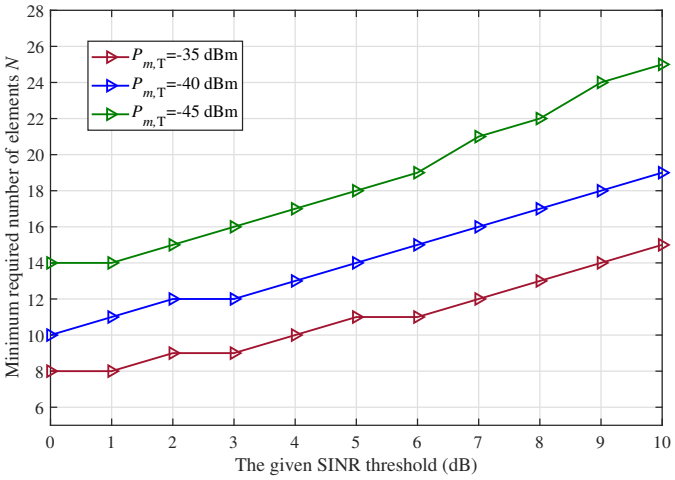

Fig. 7. The minimum required number of elements N versus the given SINR threshold for different transmit power $P_{m,\mathrm{T}}$.

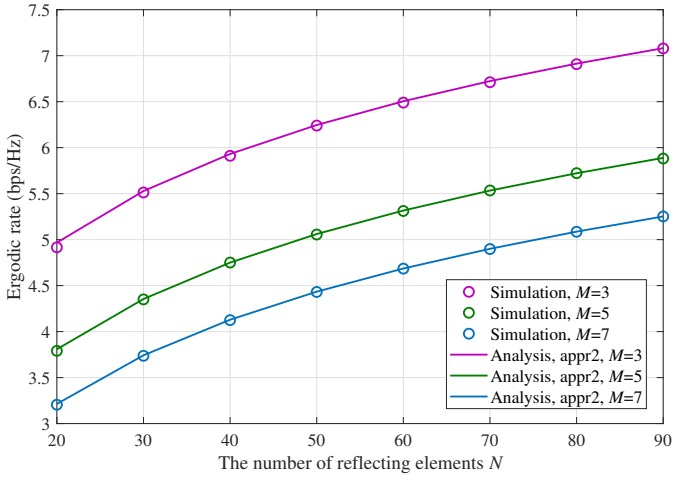

Fig. 5. The ergodic rate versus the number of reflecting elements.

modulation (QAM) ($\varphi = 2 - \frac{\sqrt{2}}{4}$, $\varsigma = \frac{3}{31}$), 16-QAM ($\varphi = \frac{3}{2}$, $\varsigma = \frac{1}{5}$), quadrature phase-shift key (QPSK) ($\varphi = 2$, $\varsigma = 1$), and binary frequency-shift keying (BFSK) ($\varphi = 1$, $\varsigma = 1$). It can be observed that the ASER decreases with the increase of the number of reflecting elements. In addition, higher-order modulation schemes yield a larger ASEP, as expected.

In Fig. 7, we investigate the minimum required number of reflecting elements versus the given SINR threshold under different values of transmit power $P_{m,\mathrm{T}}$. It can be seen that the minimum required number of reflecting elements at each IRS increases with the given SINR threshold. The main reason for this phenomenon is that more reflecting elements are needed to provide passive beamforming gain to satisfy the increasing demand for SINR. Especially, due to the fact that the number of IRS's elements is a positive integer, the growth curves in Fig. 7 are not smooth but exhibit a stepped increase. In addition, one can observe that for a fixed SINR threshold, increasing the transmit power of the HAP can significantly reduce the required minimum number of elements.

Fig. 8 shows the ergodic capacity versus the number of reflecting elements for different transmit power of the HAP. In this figure, the curves labeled 'Optimal' are obtained

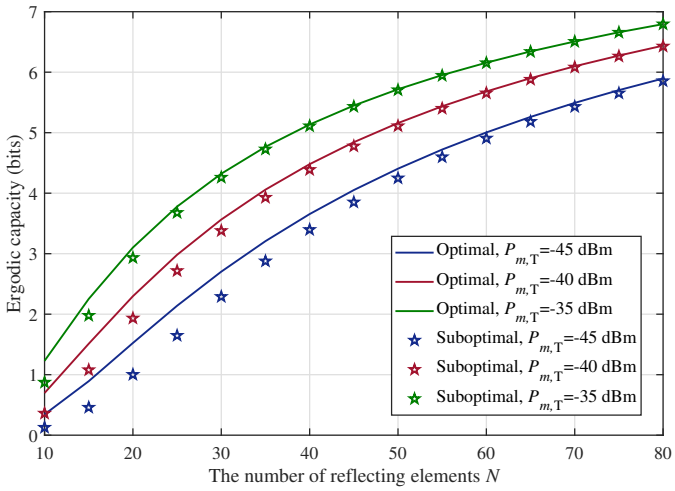

Fig. 8. The ergodic capacity versus the number of reflecting elements for different transmit power $P_{m,\mathrm{T}}$.

using exhaustive search algorithm, while the curves labeled 'Suboptimal' are derived from Lemma 6. It can be observed that the ergodic capacity performance enhances with the number of IRS's reflecting elements or the transmit power of the HAP. In particular, on can see that in regions with high values of reflecting elements, our proposed sub-optimal solution can achieve the same ergodic capacity performance as the optimal solution. This further confirms the correctness of the theoretical result we derived in Lemma 6.

VI. Conclusion

In this paper, we studied an IRS-assisted multi-cell DEIN. Specifically, the energy from neighboring cells during the downlink WET stage enhances the uplink data transmission capacity of the edge UE in the typical cell. Nevertheless, in the uplink WIT stage, co-frequency interference from neighboring cells could result in a reduction of the ergodic capacity performance for the edge UE in the typical cell. We first characterized the statistical features of the instantaneous SINR at the typical edge UE. Then, the outage probability, ergodic rate and ASEP for the edge UE in the typical cell were derived. To gain more insight, we conduct the minimum required number of IRS's reflecting elements and the sub-optimal time allocation coefficient for a given rate threshold. Finally, extensive numerical results were presented to verify the correctness of our obtained results. With the advancement of wireless communication technologies, cell-free networks are gaining increasing attention. In future work, we will further investigate the overall performance of IRS-assisted DEIN systems in cell-free massive multiple input multiple output transmission scenarios.

Appendix A
Proof of Lemma 3

Based on the definition of achievable rate in (11), the ergodic rate for the edge UE in the typical cell m can be defined as

$$R_m = \mathbb{E}\left[\log_2\left(1+\gamma_m\right)\right] = \int_0^\infty \log_2\left(1+x\right) f_{\gamma_m}(x)\mathrm{d}x. \tag{A.1}$$

Now, for the continuation of the derivation, it is necessary to obtain the PDF of γ_m. By using [37, Eq. (8.2.2.30)] and taking the first-order derivation of (29), the PDF of γ_m can be derived as

$$f_{\gamma_m}(x) = \frac{x^{-1}}{\Gamma(\beta_Z)\Gamma(\beta_L)\Gamma(\beta_I)} G_{3,4}^{2,3}\left(\frac{\theta_I x}{\theta_Z\theta_L}\left|{}^{1-\beta_I,1,0}_{\beta_L,\beta_Z,0,1}\right.\right). \tag{A.2}$$

Then, as the subsequent derivation process is similar to our previous work [41], we omit the details for simplicity.

Appendix B
Proof of Lemma 4

By substituting (A.2) in (36) and using $Q(x) = \frac{1}{2}\mathrm{erfc}\left(\frac{x}{\sqrt{2}}\right)$, one has

$$\begin{aligned}\bar{P}_e &= \frac{\varphi}{2\Gamma(\beta_Z)\Gamma(\beta_L)\Gamma(\beta_I)}\int_0^\infty t^{-1}\mathrm{erfc}\left(\sqrt{\frac{\varsigma t}{2}}\right) \\ &\quad\times G_{3,4}^{2,3}\left(\frac{\theta_I t}{\theta_Z\theta_L}\left|{}^{1-\beta_I,1,0}_{\beta_L,\beta_Z,0,1}\right.\right)\mathrm{d}t \\ &\overset{(a)}{=} \frac{\varphi}{2\sqrt{\pi}\Gamma(\beta_Z)\Gamma(\beta_L)\Gamma(\beta_I)}\int_0^\infty t^{-1}G_{1,2}^{2,0}\left(\frac{\varsigma t}{2}\left|{}^{1}_{0,\frac{1}{2}}\right.\right) \\ &\quad\times G_{3,4}^{2,3}\left(\frac{\theta_I t}{\theta_Z\theta_L}\left|{}^{1-\beta_I,1,0}_{\beta_L,\beta_Z,0,1}\right.\right)\mathrm{d}t \\ &\overset{(b)}{=} \frac{\varphi}{2\sqrt{\pi}\Gamma(\beta_Z)\Gamma(\beta_L)\Gamma(\beta_I)} G_{5,5}^{2,5}\left(\frac{2\theta_I}{\varsigma\theta_Z\theta_L}\left|{}^{1,\frac{1}{2},1-\beta_I,1,0}_{\beta_L,\beta_Z,0,1,0}\right.\right),\end{aligned} \tag{B.1}$$

where (a) follows from [37, Eq. (8.4.14.2)] and (b) is obtained by using [38, Eq. (9.31.5), Eq. (7.811.1)]. Here, the proof is completed.

Appendix C
Proof of Lemma 5

For the univariate quartic inequality in (45), we first set the inequality to equality, transforming it into a univariate quartic equation. One has

$$AN^4 + BN^3 + CN^2 + D = 0. \tag{C.1}$$

Subsequently, by employing the Ferrari method [42], one can obtain the four roots of the equation as follows:

$$x_1 = \lambda_4 - \lambda_5 - \lambda_{6a}, \tag{C.2a}$$
$$x_2 = \lambda_4 - \lambda_5 + \lambda_{6a}, \tag{C.2b}$$
$$x_3 = \lambda_4 + \lambda_5 - \lambda_{6a}, \tag{C.2c}$$
$$x_4 = \lambda_4 + \lambda_5 + \lambda_{6a}, \tag{C.2d}$$

where $\lambda_4 = -\frac{B}{4A}$, $\lambda_5 = \frac{1}{2}\sqrt{\lambda_2+\Delta_3}$, $\lambda_{6a} = \frac{1}{2}\sqrt{2\lambda_2 - \Delta_3 - \frac{\lambda_3}{8\lambda_5}}$, $\lambda_{6b} = \frac{1}{2}\sqrt{2\lambda_2 - \Delta_3 + \frac{\lambda_3}{8\lambda_5}}$, $\lambda_2 = \frac{B^2}{4A^2} - \frac{2C}{3A}$, $\lambda_3 = -\frac{B^3}{A^3} + \frac{4BC}{A^2}$, $\Delta_3 = \frac{\sqrt[3]{2}\Delta_1}{3A\lambda_1} + \frac{\lambda_1}{3\sqrt[3]{2}A}$, $\lambda_1 = \sqrt[3]{\Delta_2 + \sqrt{-4\Delta_1^3 + \Delta_2^2}}$, $\Delta_1 = C^2 + 12AD$ and $\Delta_2 = 2C^3 + 27B^2D - 72ACD$.

Due to the fact that the number of reflecting elements always a positive integer, we discard complex and negative values among the four roots obtained. Furthermore, we need to round up the positive roots to obtain the minimum required number of reflecting elements.

APPENDIX D
PROOF OF LEMMA 6

With a relatively large number of reflecting elements in the IRS, one can apply Taylor expansion to obtain

$$\ln\left(1+\frac{\varepsilon_1}{\varepsilon_2+\varepsilon_3 u_m}\right) \approx \ln\left(1+\frac{\varepsilon_1}{\varepsilon_2}\right)-\frac{\varepsilon_1\varepsilon_3 u_m}{\varepsilon_2^2\left(1+\frac{\varepsilon_1}{\varepsilon_2}\right)}+\mathcal{O}\left(u_m^2\right), \tag{D.1}$$

where ε_1, ε_2 and ε_3 are defined in (47), and $u_m=\frac{\tau^{\mathrm{I}}}{1-\tau^{\mathrm{I}}}$.

Then, by substituting (D.1) into (47), one can have

$$\begin{aligned} C_m &\approx \frac{1}{\ln 2}\frac{u_m}{1+u_m}\left[\ln\left(1+\frac{\varepsilon_1}{\varepsilon_2}\right)-\frac{\varepsilon_1\varepsilon_3 u_m}{\varepsilon_2^2\left(1+\frac{\varepsilon_1}{\varepsilon_2}\right)}\right] \\ &= \frac{\varpi_1 u_m-\varpi_2 u_m^2}{1+u_m}, \end{aligned} \tag{D.2}$$

where $\varpi_1=\frac{1}{\ln 2}\ln\left(1+\frac{\varepsilon_1}{\varepsilon_2}\right)$ and $\varpi_2=\frac{1}{\ln 2}\frac{\varepsilon_1\varepsilon_3}{\varepsilon_2^2\left(1+\frac{\varepsilon_1}{\varepsilon_2}\right)}$.

By taking the derivative of C_m in (D.2) w.r.t. u_m, one has

$$C_m^{'}=\frac{\varpi_1-2\varpi_2 u_m-\varpi_2 u_m^2}{\left(1+u_m\right)^2}. \tag{D.3}$$

Let $C_m^{'}=0$, that is $\varpi_1-2\varpi_2 u_m-\varpi_2 u_m^2=0$. For the above univariate quadratic equation, one can easily prove that its discriminant $\Delta=4\varpi_2^2+4\varpi_1\varpi_2>0$. As a result, on can obtain two solutions to this equation as [43]

$$x_1=\frac{-2\varpi_2+\sqrt{4\varpi_2^2+4\varpi_1\varpi_2}}{2\varpi_2}>0, \tag{D.4a}$$

$$x_2=\frac{-2\varpi_2-\sqrt{4\varpi_2^2+4\varpi_1\varpi_2}}{2\varpi_2}<0. \tag{D.4b}$$

Because u_m needs to satisfy $u_m>0$, x_2 is discarded. Finally, based on (D.4a) and $\tau^{\mathrm{I}}=\frac{u_m}{1+u_m}$, (48) can be obtained by simple variable substitution. Here, this proof is complete.

REFERENCES

[1] C.-X. Wang, X. You, X. Gao, X. Zhu, Z. Li, C. Zhang, H. Wang, Y. Huang, Y. Chen, H. Haas, J. S. Thompson, E. G. Larsson, M. D. Renzo, W. Tong, P. Zhu, X. Shen, H. V. Poor, and L. Hanzo, "On the road to 6G: Visions, requirements, key technologies, and testbeds," *IEEE Commun. Surveys Tuts.*, vol. 25, no. 2, pp. 905–974, 2023.

[2] J. Hu, K. Yang, G. Wen, and L. Hanzo, "Integrated data and energy communication network: A comprehensive survey," *IEEE Commun. Surveys Tuts.*, vol. 20, no. 4, pp. 3169–3219, 2018.

[3] J. Zheng, J. Zhang, and B. Ai, "UAV communications with WPT-aided cell-free massive MIMO systems," *IEEE J. Sel. Areas Commun.*, vol. 39, no. 10, pp. 3114–3128, 2021.

[4] N. Guo, X. Yuan, Y. Hu, and A. Schmeink, "Reliability-oriented resource allocation for wireless powered short packet communications with multiple WPT sources," *IEEE Trans. Wireless Commun.*, vol. 22, no. 12, pp. 8983–8998, 2023.

[5] X. Fan, J. Hu, Y. Zhao, and K. Yang, "Distributed batteryless access control for data and energy integrated networks: Modeling and performance analysis," *IEEE Internet Things J.*, vol. 10, no. 15, pp. 13 428–13 441, 2023.

[6] N. Shanin, A. Hagelauer, L. Cottatellucci, and R. Schober, "Optimal energy signal design for multiuser MISO WPCNs with non-linear energy harvesting circuits," *IEEE Trans. Commun.*, vol. 71, no. 6, pp. 3402–3418, 2023.

[7] H. Hu, K. Xiong, H.-C. Yang, P. Fan, and K. B. Letaief, "Age of information analysis of WPCN over rician fading channel with non-linear penalty," *IEEE Internet Things J.*, pp. 1–1, 2023.

[8] C. Pan, H. Ren, K. Wang, J. F. Kolb, M. Elkashlan, M. Chen, M. Di Renzo, Y. Hao, J. Wang, A. L. Swindlehurst, X. You, and L. Hanzo, "Reconfigurable intelligent surfaces for 6G systems: Principles, applications, and research directions," *IEEE Commun. Mag.*, vol. 59, no. 6, pp. 14–20, 2021.

[9] Q. Wu and R. Zhang, "Towards smart and reconfigurable environment: Intelligent reflecting surface aided wireless network," *IEEE Commun. Mag.*, vol. 58, no. 1, pp. 106–112, 2020.

[10] H. Wang, Z. Zhang, B. Zhu, J. Dang, and L. Wu, "Optical reconfigurable intelligent surfaces aided optical wireless communications: Opportunities, challenges, and trends," *IEEE Wireless Commun.*, vol. 30, no. 5, pp. 28–35, 2023.

[11] Z. Peng, X. Chen, C. Pan, M. Elkashlan, and J. Wang, "Performance analysis and optimization for RIS-assisted multi-user massive MIMO systems with imperfect hardware," *IEEE Trans. Veh. Technol.*, vol. 71, no. 11, pp. 11 786–11 802, 2022.

[12] W. Mei and R. Zhang, "Performance analysis and user association optimization for wireless network aided by multiple intelligent reflecting surfaces," *IEEE Trans. Commun.*, vol. 69, no. 9, pp. 6296–6312, 2021.

[13] J. Lyu and R. Zhang, "Hybrid active/passive wireless network aided by intelligent reflecting surface: System modeling and performance analysis," *IEEE Trans. Wireless Commun.*, vol. 20, no. 11, pp. 7196–7212, 2021.

[14] A. Bansal, K. Singh, B. Clerckx, C.-P. Li, and M.-S. Alouini, "Rate-splitting multiple access for intelligent reflecting surface aided multi-user communications," *IEEE Trans. Veh. Technol.*, vol. 70, no. 9, pp. 9217–9229, 2021.

[15] Z. Huang, B. Zheng, and R. Zhang, "Transforming fading channel from fast to slow: Intelligent refracting surface aided high-mobility communication," *IEEE Trans. Wireless Commun.*, vol. 21, no. 7, pp. 4989–5003, 2022.

[16] M. A. Al-Jarrah, E. Alsusa, A. Al-Dweik, and M.-S. Alouini, "Performance analysis of wireless mesh backhauling using intelligent reflecting surfaces," *IEEE Trans. Wireless Commun.*, vol. 20, no. 6, pp. 3597–3610, 2021.

[17] X. Liu, Y. Liu, and Y. Chen, "Machine learning empowered trajectory and passive beamforming design in UAV-RIS wireless networks," *IEEE J. Sel. Areas Commun.*, vol. 39, no. 7, pp. 2042–2055, 2021.

[18] D. Zhang, M. Xiao, Z. Pang, L. Wang, and H. V. Poor, "IRS assisted federated learning: A broadband over-the-air aggregation approach," *IEEE Trans. Wireless Commun.*, vol. 23, no. 5, pp. 4069–4082, 2024.

[19] H. Ren, K. Wang, and C. Pan, "Intelligent reflecting surface-aided URLLC in a factory automation scenario," *IEEE Trans. Commun.*, vol. 70, no. 1, pp. 707–723, 2022.

[20] R. Hashemi, S. Ali, N. H. Mahmood, and M. Latva-aho, "Average rate and error probability analysis in short packet communications over RIS-aided URLLC systems," *IEEE Trans. Veh. Technol.*, vol. 70, no. 10, pp. 10 320–10 334, 2021.

[21] S. Sun, F. Yang, J. Song, and Z. Han, "Joint resource management for intelligent reflecting surface–aided visible light communications," *IEEE Trans. Wireless Commun.*, vol. 21, no. 8, pp. 6508–6522, 2022.

[22] S. Aboagye, T. M. N. Ngatched, O. A. Dobre, and A. R. Ndjiongue, "Intelligent reflecting surface-aided indoor visible light communication systems," *IEEE Commun. Lett.*, vol. 25, no. 12, pp. 3913–3917, 2021.

[23] Y. Gao, Q. Wu, G. Zhang, W. Chen, D. W. K. Ng, and M. D. Renzo, "Beamforming optimization for active intelligent reflecting surface-aided SWIPT," *IEEE Trans. Wireless Commun.*, vol. 22, no. 1, pp. 362–378, 2023.

[24] P. Chen, B. Lyu, Y. Liu, H. Guo, and Z. Yang, "Multi-IRS assisted wireless-powered mobile edge computing for Internet of Things," *IEEE Trans. Green Commun. Netw.*, vol. 7, no. 1, pp. 130–144, 2023.

[25] C. Pan, H. Ren, K. Wang, M. Elkashlan, A. Nallanathan, J. Wang, and L. Hanzo, "Intelligent reflecting surface aided MIMO broadcasting for simultaneous wireless information and power transfer," *IEEE J. Sel. Areas Commun.*, vol. 38, no. 8, pp. 1719–1734, 2020.

[26] F. E. Bouanani, S. Muhaidat, P. C. Sofotasios, O. A. Dobre, and O. S. Badarneh, "Performance analysis of intelligent reflecting surface aided wireless networks with wireless power transfer," *IEEE Commun. Lett.*, vol. 25, no. 3, pp. 793–797, 2021.

[27] H. Ma, H. Zhang, Y. Zhu, and Y. Qian, "Wireless powered intelligent reflecting surface for improving broadcasting channels," *IEEE Trans. Wireless Commun.*, vol. 22, no. 4, pp. 2760–2774, 2023.

[28] M. Fu, W. Mei, and R. Zhang, "Multi-active/passive-irs enabled wireless information and power transfer: Active IRS deployment and performance analysis," *IEEE Commun. Lett.*, vol. 27, no. 8, pp. 2217–2221, 2023.

[29] T. Ji, M. Hua, C. Li, Y. Huang, and L. Yang, "Exploiting intelligent reflecting surface for enhancing full-duplex wireless-powered communication networks," *IEEE Trans. Commun.*, vol. 72, no. 1, pp. 553–569, 2024.

[30] Z. Feng, B. Clerckx, and Y. Zhao, "Waveform and beamforming design for intelligent reflecting surface aided wireless power transfer: Single-user and multi-user solutions," *IEEE Trans. Wireless Commun.*, vol. 21, no. 7, pp. 5346–5361, 2022.

[31] Q. Wu, X. Zhou, and R. Schober, "IRS-assisted wireless powered NOMA: Do we really need different phase shifts in DL and UL?" *IEEE Wireless Commun. Lett.*, vol. 10, no. 7, pp. 1493–1497, 2021.

[32] Q. Wu, X. Zhou, W. Chen, J. Li, and X. Zhang, "IRS-aided WPCNs: A new optimization framework for dynamic IRS beamforming," *IEEE Trans. Wireless Commun.*, vol. 21, no. 7, pp. 4725–4739, 2022.

[33] G. Chen, Q. Wu, W. Chen, D. W. K. Ng, and L. Hanzo, "Irs-aided wireless powered mec systems: Tdma or noma for computation offloading?" *IEEE Trans. Wireless Commun.*, vol. 22, no. 2, pp. 1201–1218, 2023.

[34] Z. Shi, H. Wang, Y. Fu, X. Ye, G. Yang, and S. Ma, "Outage performance and AoI minimization of HARQ-IR-RIS aided IoT networks," *IEEE Trans. Commun.*, vol. 71, no. 3, pp. 1740–1754, 2023.

[35] B. Zhang, K. Yang, K. Wang, and G. Zhang, "Performance analysis for RIS-assisted SWIPT-enabled IoT systems," *IEEE Trans. Wireless Commun.*, vol. 23, no. 8, pp. 10 030–10 043, 2024.

[36] B. Zhang, K. Wang, K. Yang, and G. Zhang, "IRS-assisted short packet wireless energy transfer and communications," *IEEE Wireless Commun. Lett.*, vol. 11, no. 2, pp. 303–307, 2022.

[37] A. P. Prudnikov, Y. A. Brychkov, and O. I. Marichev, *Integrals and series: Vol. 3: More special functions*. New York: CRC Press, 1992.

[38] I. S. Gradshteyn and I. M. Ryzhik, *Table of Integrals, Series, and Products,* 7th. San Diego, CA: Academic Press, 2007.

[39] M. Abramowitz and I. A. Stegun, *Handbook of mathematical functions: with formulas, graphs, and mathematical tables*. NY, USA: Dover, 1972.

[40] Y. Deng, L. Wang, M. Elkashlan, K. J. Kim, and T. Q. Duong, "Generalized selection combining for cognitive relay networks over nakagami-m fading," *IEEE Trans. Signal Process.*, vol. 63, no. 8, pp. 1993–2006, 2015.

[41] B. Zhang, K. Yang, and K. Wang, "Performance analysis of IRS-assisted and wireless power transfer enabled ISAC systems," in *Proc. IEEE Global Commun. Conf.*, 2023, pp. 1012–1017.

[42] "Quartic_function." [Online]. Available: https://mathworld.wolfram.com/QuarticEquation.html

[43] "Quadratic equation." [Online]. Available: https://en.wikipedia.org/wiki/Quadratic_equation

Bingxin Zhang (Member, IEEE) received his Ph.D. degree from the School of Information and Communication Engineering, University of Electronic Science and Technology of China, Chengdu, China, in 2024. He is currently a postdoctoral researcher with the School of Intelligent Software and Engineering, Nanjing University (Suzhou Campus), Suzhou, China. His research interests include ultra-reliable low-latency communications (URLLC), data and energy integrated communication networks (DEIN) and intelligent reflecting surface (IRS).

Kun Yang (Fellow, IEEE) received his Ph.D. from the Department of Electronic & Electrical Engineering of University College London (UCL), UK. He is currently a Chair Professor of Nanjing University, China and University of Essex, UK. His main research interests include wireless networks and communications, communicationcomputing cooperation, and new AI (artificial intelligence) for wireless. He has published 500+ papers and filed 50 patents. He serves on the editorial boards of a number of IEEE journals (e.g., IEEE WCM, TVT, TNB). He is a Deputy Editor-in-Chief of IET Smart Cities Journal. He has been a Judge of GSMA GLOMO Award at World Mobile Congress-Barcelona since 2019. He was a Distinguished Lecturer of IEEE ComSoc (2020-2021), a Recipient of the 2024 IET Achievement Medals and the Recipient of 2024 IEEE CommSoft TC's Technical Achievement Award. He is a Member of Academia Europaea (MAE), a Fellow of IEEE, a Fellow of IET and a Distinguished Member of ACM.

Kezhi Wang (Senior Member, IEEE) received the Ph.D. degree from the University of Warwick, U.K. He is currently a Professor with the Department of Computer Science, Brunel University London, U.K. His research interests include wireless communications, mobile edge computing, and machine learning. He is a Royal Society Industry Fellow and a Clarivate Highly Cited Researcher in 2023-2024.

Guopeng Zhang received the Ph.D. degree from the School of Communication Engineering, Xidian University, Xi'an, China, in 2009. He is currently a Professor with the School of Computer Science and Technology, China University of Mining and Technology, Xu'zhou, China. He has authored or co-authored more than 60 journal and conference papers. His main research interests include distributed machine learning, data mining, and mobile edge computing.